ResearchGate

See discussions, stats, and author profiles for this publication at: https://www.researchgate.net/publication/228643539

Tip leakage flows in turbines

Article · January 2006

CITATIONS
10

READS
4,454

1 author:

Piotr Lampart
Institute of Fluid Flow Machinery
90 PUBLICATIONS **402** CITATIONS

SEE PROFILE

All content following this page was uploaded by Piotr Lampart on 26 May 2014.

The user has requested enhancement of the downloaded file.

TASK QUARTERLY 10 No 2, 139–175

TIP LEAKAGE FLOWS IN TURBINES

PIOTR LAMPART

Institute of Fluid-Flow Machinery,
Polish Academy of Sciences,
Fiszera 14, 80-952 Gdansk, Poland
lampart@imp.gda.pl

(Received 7 February 2006; revised manuscript received 12 March 2006)

Abstract: Mechanisms of formation of the tip leakage over shrouded and unshrouded rotor blades are described in the paper. The loss diagrams for these two types of leakage in a wide range of cascade inlet and outlet flow angles are also plotted. They are obtained in a theoretical way from a model of stream mixing with the help of simplifying assumptions concerning the load of the rotor profile. Results of numerical investigations based on a 3D RANS solver FlowER are also presented in the paper. They extend on the effects of geometrical and flow parameters of the cascade (stage or stage group) on the development of flow losses in the leakage-dominated region as well as on the interaction of tip leakage flow with secondary flows. The tip clearance size, the level of flow turning in the cascade, incidence angle and the effect of relative motion of the blades and endwall are considered here in the case of unshrouded free-tip blades. In the case of shrouded rotor blades the tip leakage mass flow rate and its direction on the re-entry to the blade-to-blade passage. Since the tip leakage non-uniformities are hardly dissipated within the blade row where they originate, the interaction of the tip leakage with the flow in the downstream stator is considered. Some investigations also take into account the effect of relative motion of the stator and rotor blades.

Keywords: axial flow turbine, shrouded/unshrouded blades, tip leakage, CFD

1. Introduction

Side flows are inherent to turbomachinery as they result from the presence of technological clearances between the fixed and rotating parts of machinery. Among different types of side flows are leakage flows over the rotor and stator blade tips of unshrouded blades, labyrinth flows over shrouded rotor blades and through stator root seals, windage flows at the rotor disc and discharge flows through the rotor disc discharge holes. A sample diagram of distribution of flow into the blade-to-blade passages and leakage flow clearances for a group of high-pressure (HP) stages of an impulse steam turbine with shrouded rotor blades is presented in Figure 1. Leakage streams bypass the blade-to-blade passage and do not yield work to the rotor. Therefore, they are sources of power loss in turbines.

In this paper the attention is focused on the main form of leakage flow, that is the tip leakage over the rotating rotor blade. The tip leakage is characterised by parameters different than those of the main stream, which is documented by

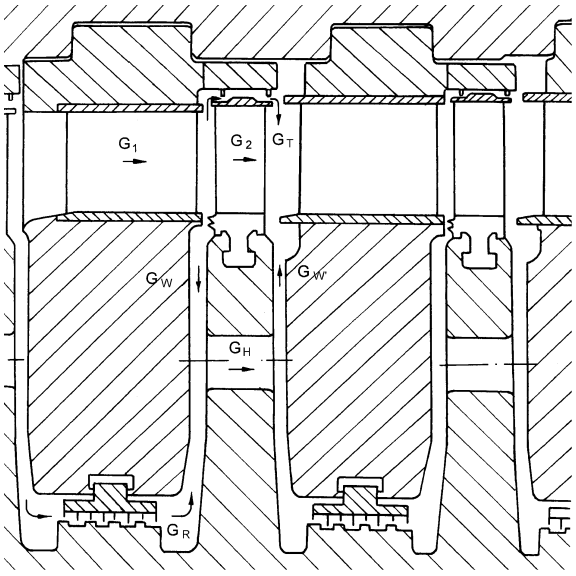

Figure 1. Impulse turbine geometry; G_1, G_2 – mass flow rates of the main flow in the blade-to-blade passage of the stator and rotor, G_T, G_R – flow rates of leakages at the rotor blade tip and stator root, G_W, $G_{W'}$ – windage flow rates at the rotor disc, G_H – flow rate at the rotor disc discharge holes

measurements on large-scale turbines, *e.g.* [1] or [2]. Particularly important is the difference between the magnitudes and directions of the leakage flow and main stream velocities, which gives rise to mixing losses on the re-entry of the leakage stream to the blade-to-blade passage. It is also important to note that the mechanism of formation of the tip leakage over unshrouded free-tip blades is different than that of leakage over shrouded blades, [3]. Therefore, these two types of leakage need to be considered separately.

2. Formation of tip leakage over unshrouded rotor blades

The mechanism of formation of the tip leakage in the gap over unshrouded rotor blades and its further development in the blade-to-blade passage is illustrated in Figure 2. The driving force for this type of leakage is the pressure difference that is formed over the blade tip between the pressure and suction surface of the blade. Due to a usually significant pressure gradient, the leakage stream is largely accelerated in the tip gap. In the transonic cascades, the tip leakage stream reaches supersonic velocities that can be compared to those at the blade suction surface in the blade-to-blade passage. At the entrance to the tip gap, the tip leakage typically separates from the sharp edge of the blade tip. The tip leakage is contracted into a narrow stream between the separation region and endwall. Here, the leakage stream becomes turbulent and mixes with the shear layer separating it from the stagnation area. Downstream, the leakage jet fills the entire tip gap and further mixing takes place to equalise flow non-uniformities in the leakage stream. Downstream of the gap the tip leakage faces the adverse pressure gradient in the channel and separates from the endwall forming a vortex structure that is convected downstream, [4–6]. A detailed investigation of

the leakage stream in the tip gap is the subject of the paper [7]. The tip leakage flow is not turned in the blade-to-blade passage in a way the main stream is. The tip leakage follows the pressure gradient across the tip gap, so its direction on the re-entry to the blade-to-blade passage usually forms an oblique angle with the main stream direction.

In [8], some effects are identified of the tip gap flow on the distribution of static pressure at the endwall, which largely remains similar to that formed in the blade-to-blade passage, except for the gap region over the blade tip. This refers both to the situation of fixed (non-rotating) blades and endwall as well as to the case of relative motion between the blade tip and endwall[1]. The main difference is a region of decreased pressure over the blade tip edge. This is a relatively small pressure decrease above the pressure surface and a more considerable pressure decrease above the suction surface, that is at the entry from the tip gap. This redistribution of pressure around the blade tip results in a change of load of the blade tip. Typically, there is a minor change in circumferential force that gives the rotational moment. More significant are changes in axial force, where typically an increase of about 5–10% depending on the cascade geometry and tip gap size is observed, as compared to the cascade without a tip clearance. These effects were documented by [6, 9–11].

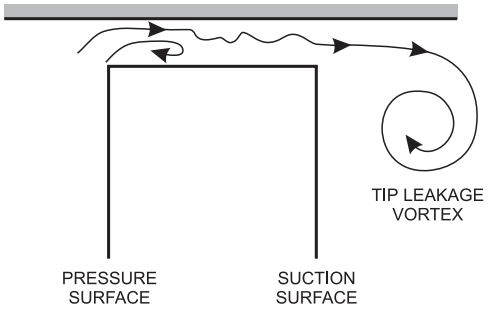

Figure 2. Scheme of the tip leakage over unshrouded rotor blades

The presence of the tip gap over the blade usually eliminates the stagnation at the endwall, which typically occurs in the corner between the endwall and blade leading edge in the no tip gap configuration. Therefore, a horseshoe vortex does not feature at the tip endwall unless the tip gap is very small. The flow at the tip endwall approaching the tip region above the leading edge of the blade is divided into two streams aiming towards low pressure regions above the suction surfaces of the neighbouring blades – a main stream of the tip leakage flow going through the tip gap over the blade and a stream of cross-flow going across the blade-to-blade passage [12]. The tip leakage flow leaving the tip gap separates from the endwall

1. Over the years, knowledge of the physics of tip leakage flow has mainly been acquired from results of experimental investigations of model cascades with a tip clearance. Most of these investigations were made on stationary cascades, only some investigations taking into account the relative motion of blade tips and endwalls. Investigations in a fully stationary environment enabled detailed measurements and thorough tracing of flow patterns, wheras taking into account the relative motion assures the relevance of the experiment to real turbomachinery situations.

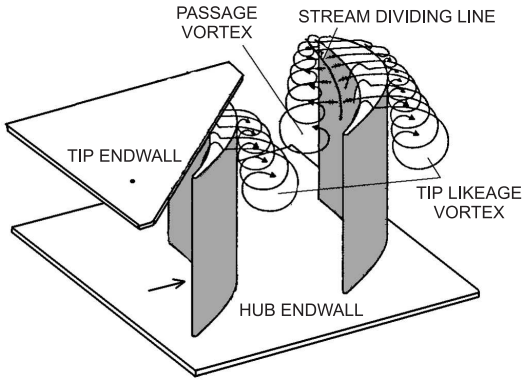

Figure 3. Tip leakage vortex and passage vortex at the tip endwall

under conditions of adverse pressure gradient and forms the tip leakage vortex. The cross-flow blocked by the development of the tip leakage vortex also separates from the endwall and rolls up into a passage vortex. The stream dividing line between the tip leakage and cross-passage flow lies at the pressure side of the blade tip, [13]. The described situation is illustrated in Figure 3. The tip leakage vortex and passage vortex are characterised by the opposite sense of rotation. It follows from [14–16] that a dominant structure is the tip leakage vortex. The relations between the circulation and size of the two structures depend on many factors including the tip gap size, flow turning angle, blade load and incidence angle. For a typical low-load rotor cascades for the nominal inflow and typical tip gap size ranging between 1–3%, the circulation of the tip leakage vortex is several times larger than that of the passage vortex.

Interaction of the tip leakage vortex and passage vortex is a complex process. In high-turning turbine cascades investigated in [17–19], as a result of shear interaction with the larger tip leakage vortex, the passage vortex is moved towards mid-span sections, its structure elongated and circulation reduced. The circulation of the passage vortex changes with the incidence at the blade and is largely decreased when the incidence is moved towards the suction side, that is when the flow turning in the cascade is reduced. At the same time the circulation of the tip leakage vortex practically remains unchanged with the changing incidence angle, however, exhibits significant changes with the increasing tip gap width. The investigations of a low-turning cascade presented in [20] show that the weaker passage vortex is quickly dissipated. The remains of vorticity of the sense of rotation the same as that of the passage vortex are observed at the endwall/pressure surface corner near the separation of cross-flow from the endwall.

The tip leakage region is characterised by a high level of flow turbulence. Production of turbulent kinetic energy and its dissipation is a significant source of flow losses. The results of detailed measurements presented in [21] indicate the turbulence intensity of 30% (with respect to the inlet velocity) in the region of separation of the tip leakage flow from the endwall, in the tip leakage vortex and passage vortex as well as in the region of high stress resulting from interaction of the two vortex structures. The turbulence intensity of the leakage stream in the tip gap exceeds locally 26% (with respect to the outlet velocity), [22].

3. Tip leakage loss diagram for unshrouded blades

In general, enthalpy losses due to tip leakage over unshrouded rotor blades are losses of friction and mixing of streams. Neglecting the effect of viscous forces on the process of formation of the tip leakage vortex, or in other words assuming that its formation is predominantly conditioned by the action of pressure and inertia forces, the following basic loss mechanisms in the tip leakage region can be enumerated:

1. friction of the leakage stream against the blade tip and endwall;
2. shear effects in the non-uniform leakage stream within the tip gap, including the region of separation of the leakage stream from the blade tip edge;
3. shear effects in the region of division of the tip leakage vortex and passage vortex and at the suction side of the blade in the region of influence of the tip leakage vortex;
4. dissipation of secondary energy associated with the tip leakage vortex in the process of its mixing with the main flow and with other types of vortex flows. As in the case of passage vortex, the entire secondary energy of the tip leakage vortex can be assumed lost during the mixing;
5. the presence of tip clearance and the relative motion of the blade tips and endwall change the development of secondary flows and cause a redistribution of secondary flow losses. In the presence of tip leakage, secondary flow losses are usually lower than in an analogical cascade without the tip gap;
6. the mixing processes due to tip leakage are usually not accomplished in the current blade row and are continued in a subsequent stator blade row located downstream. Significant discrepancies in the distribution of exit velocity and swirl angle between the main flow and the tip region lead to a non-nominal incidence at the downstream stator blade in the tip region, which is usually a source of additional downstream blade losses, [23]. In some exceptional cases of low-load, low-turning cascades at very low tip gap sizes and relatively large axial distance between the subsequent stages, flow losses in the downstream blade row may not change or even be lower than in the case of no tip gap, [24, 25]. This situation can occur if the incidence at the downstream stator blade moved in the tip leakage region towards the suction surface still remains in the near-nominal range, whereas the locally reduced flow turning in the blade-to-blade passage in the tip leakage region acts to reduce the profile and secondary flow losses.

The total loss at the tip endwall is decomposed according to the formula [26]:

$$Y_{end(tip)} = Y_{gap} + k_s Y_{sec,0} + Y_{tip} \tag{1}$$

where Y_{gap} denotes tip leakage losses inside the tip gap, $Y_{sec,0}$ – secondary flow losses at zero tip gap size, Y_{tip} – tip leakage losses outside the tip gap, that is in the blade-to-blade passage of the current and downstream rows. Usually the third factor of this decomposition is dominant. Out of the three loss components, the evaluation of flow losses inside the tip gap is relatively simple. The separation of the remaining loss components is not that easy. It is evaluated in [5, 12] that the tip leakage losses within the tip gap account for 0.20 of the total endwall losses (including both secondary and tip leakage losses) for a 2% tip gap and decrease with the increasing tip gap size. The contribution of secondary flow losses is found to depend on the tip gap size, which is

accounted for in the form of the coefficient k_s in Equation (1), ranging between zero and unity and decreasing with the increasing tip gap size. The decomposition of the total endwall loss is tentatively illustrated in Figure 4 borrowed from experimental investigations presented in [26]. The diagram was made for the case of a cascade with the tip clearance but without taking into account the effect of relative motion of the blade tips and endwall. With the relative motion, one can expect a certain increase of the loss component within the tip gap due to increased stresses between the leakage stream and endwall in the relative motion.

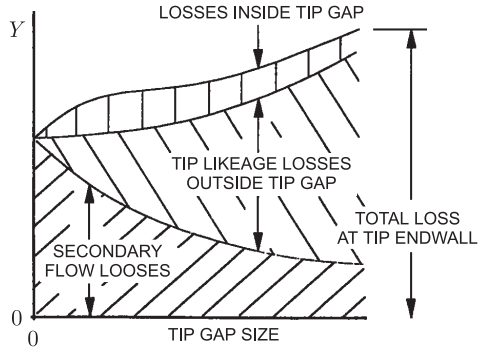

Figure 4. Tentative diagram of contribution of loss components in the total endwall loss [26]

The size of the tip gap (relative to the channel height) is of primary importance for the level of tip leakage losses, which is accounted for in all experimental and theoretical tip leakage loss correlations, *e.g.* [26–29]. A linear relationship is usually assumed, which is supported by the results of experimental investigations presented in [5, 26]. The correlations also take into account the effects of flow turning in the cascade and its density (pitch-to-chord ratio).

Enthalpy losses due to the tip leakage over unshrouded rotor blades can be estimated following the procedure described in [3] based on a model of mixing of non-parallel streams or a model of lost kinetic energy of the tip leakage flow relative to the main flow, and making use of some simplified assumptions concerning the blade load. The obtained final results may vary depending on the assumed model of mixing and blade load simplifications. Denton neglects the mixing within the tip gap and assumes that the mixing takes places at the suction surface of the blade, at a constant volume and pressure. The main stream is the flow at the suction surface of velocity $V_1 = V_s$, Figure 5. Assuming that the static pressure of the tip leakage is the same as that of the main stream at the suction surface, that is $p_j = p_1 = p_s$, and neglecting any total pressure losses of the tip leakage and main stream until the area of mixing, one can obtain that the leakage stream velocity is equal to that of the main stream, $V_j = V_1 = V_s$. Denton also assumes that the streamwise velocity component of the tip leakage is equal to the main flow velocity at the pressure surface V_p, from where the tip leakage flow originates, and that further acceleration of the tip leakage in the tip gap takes place in the direction normal to the flow. This enables the determination of velocity components of the main flow and tip leakage as the entry conditions for the

mixing process in the coordinate system along the streamwise, cross-flow and radial direction, respectively:

$$V_1 = [V_s, 0, 0], \quad V_j = \left[V_p, \sqrt{V_s^2 - V_p^2}, 0\right]. \tag{2}$$

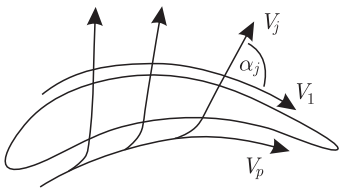

Figure 5. Model of mixing in the region of tip leakage over an unshrouded rotor blade [3]

The loss coefficient due to mixing of the tip leakage with the main stream, found from the condition of lost kinetic energy of the relative flow of the tip leakage can be evaluated as follows:

$$\begin{aligned} \xi &= \int_C \frac{dm_j}{m_2}\frac{e_{rel}}{e_2} = \int_C \frac{dm_j}{m_2}\frac{V_{rel}^2}{V_2^2} \approx \int_C \frac{dm_j}{m_1}\frac{V_{rel}^2}{V_1^2} \\ &= \int_C \frac{dm_j}{m_1}\frac{(V_s - V_p)^2 + \left(V_s^2 - V_p^2\right)}{V_s^2} = \int_C \frac{dm_j}{m_1} 2\left(1 - \frac{V_p}{V_s}\right), \end{aligned} \tag{3}$$

with the integral along the profile chord C. The symbol m denotes the mass flow rate, e is the kinetic energy. Subscripts 1, j, 2 stand for the main stream, leakage stream and mixed-out stream, respectively. Subscripts s, p denote the suction and pressure side. It is assumed that the mass flow rate of the leakage stream is small with respect to that of the main or mixed-out stream ($m_j \ll m_1$).

The mass flow rate of the main stream in Equation (3) can be found from the formula:

$$m_1 = \rho h p V_x, \tag{4}$$

whereas the elementary mass flow rate of the leakage stream can be described as:

$$dm_j = \rho V_{jn} C_\delta \delta dC = \rho \sqrt{V_s^2 - V_p^2}\, C_\delta \delta dC, \tag{5}$$

where h is the blade height, p – cascade pitch, dC – the profile chord element, δ – tip gap size, C_δ – contraction coefficient for the tip leakage stream that expresses the effect of partial blockage of the tip gap by the separation from the blade tip edge and by the endwall boundary layer. V_x denotes the axial component of the main flow velocity, V_{jn} is the velocity component of the leakage flow normal to the main flow. Thus, the loss coefficient takes the form:

$$\xi = Y = \frac{2C_\delta \delta}{h}\frac{C}{p}\int_0^1 \frac{V_s - V_p}{V_x}\sqrt{1 - \frac{V_p^2}{V_s^2}}\, dx, \tag{6}$$

which can further be transformed with the help of simplifying assumptions about the chordwise distribution of the profile load. Let us assume the model of a thin profile with a constant load (constant suction and pressure surface velocity difference) along the chord, $V_s - V_p = 2\Delta V = \text{const}$, with the mean surface velocity $\overline{V} = (V_s + V_p)/2$

linked to the axial velocity by the formula $\overline{V}\cos\alpha = V_x$, where α is the current flow angle changing between the inlet and exit angle α_0, α_1[2], respectively. The surface velocity difference can be linked to the pitch-to-chord ratio p/C, whose reverse appears in Equation (6), using the conservation equation for the circumferential component of the momentum in blade-to-blade passage (neglecting the boundary layer losses):

$$\int_0^1 \rho C\left(\frac{V_s^2}{2}-\frac{V_p^2}{2}\right)\cos\alpha dx = \rho p V_x^2(\mathrm{tg}\,\alpha_1-\mathrm{tg}\,\alpha_0),\ \Rightarrow\ p/C = \frac{2\Delta V}{V_x(\mathrm{tg}\,\alpha_1-\mathrm{tg}\,\alpha_0)}, \quad (7)$$

which turns Equation (6) into

$$\begin{aligned}\xi = Y &= \frac{2C_\delta\delta}{h}(\mathrm{tg}\,\alpha_1-\mathrm{tg}\,\alpha_0)\int_0^1\sqrt{1-\frac{V_p^2}{V_s^2}}dx\\ &= \frac{2C_\delta\delta}{h}(\mathrm{tg}\,\alpha_1-\mathrm{tg}\,\alpha_0)\int_0^1\sqrt{1-\frac{(-\Delta V/V_x+1/\cos\alpha)^2}{(\Delta V/V_x+1/\cos\alpha)^2}}dx.\end{aligned} \quad (8)$$

A further assumption can be made that $\mathrm{tg}\,\alpha$ changes linearly with x. An expression for the optimum value of the pitch-to-chord ratio or $\Delta V/V_x$ corresponding to the case of minimum loss coefficient for the blade boundary layer can also be utilised. As shown in [27], the minimum profile boundary layer loss for the assumed blade load distribution occurs at $\Delta V/V_x = \sqrt{c_1/3c_2}$, yielding the following formula for the tip leakage loss coefficient:

$$\xi = \frac{2C_\delta\delta}{h}\int_{\mathrm{tg}\,\alpha_0}^{\mathrm{tg}\,\alpha_1}\sqrt{1-\frac{\left(-\sqrt{c_1/3c_2}+\sqrt{1+x^2}\right)^2}{\left(\sqrt{c_1/3c_2}+\sqrt{1+x^2}\right)^2}}dx, \quad (9)$$

where

$$\begin{aligned}c_1 &= \frac{1}{4}\left(\frac{\mathrm{tg}\,\alpha_1}{\cos^3\alpha_1}-\frac{\mathrm{tg}\,\alpha_0}{\cos^3\alpha_0}+3c_2\right),\\ c_2 &= \frac{1}{2}\left(\frac{\mathrm{tg}\,\alpha_1}{\cos\alpha_1}-\frac{\mathrm{tg}\,\alpha_0}{\cos\alpha_0}+\ln\frac{\mathrm{tg}\,\alpha_1+\frac{1}{\cos\alpha_1}}{\mathrm{tg}\,\alpha_0+\frac{1}{\cos\alpha_0}}\right).\end{aligned} \quad (10)$$

Equation (9) can be integrated numerically for given pairs of cascade inlet and exit angles.

The contraction coefficient C_δ varies typically between 0.6 and 0.8 in the case of no relative motion of the blade tips and endwall, [3, 30, 31]. For the case of relative motion corresponding to the nominal rotational speed of the rotor blade, the value of the contraction coefficient obtained in [32] is decreased to 0.45. In [3], it is suggested that the contraction coefficient for the case of relative motion the blade tips and endwall should be reduced twice as compared to that of no relative motion. In [33], the basic value of the contraction coefficient for the case of relative motion is assumed as 0.3, however this value is corrected on non-nominal operating conditions according to the method presented in [34].

2. The circumferential (swirl) angle is measured here from the projection of the turbine axis in the blade-to-blade plane.

The diagram of the tip leakage loss coefficient for unshrouded blades as a function of cascade inlet and exit angles α_0, α_1 is presented in Figure 6. The diagram was plotted based on Equation (9) for the 1% tip gap size, assuming the contraction coefficient as $C_\delta = 0.4$. The tip leakage losses can change in a wide range depending on the cascade inlet and exit angles. For a combination of inlet and exit angles typical for the rotor cascade of the reaction stage $\alpha_0 = (-20^\circ, 20^\circ)$, $\alpha_1 = (70^\circ, 75^\circ)$, the calculated loss coefficient ranges between 1.9–3.3%. In the case of a typical impulse stage, that is $\alpha_0 = (-65^\circ, -60^\circ)$, $\alpha_1 = (65^\circ, 75^\circ)$, the calculated loss coefficient changes within 2.9–4.9% for every 1% tip gap size relative to the channel height.

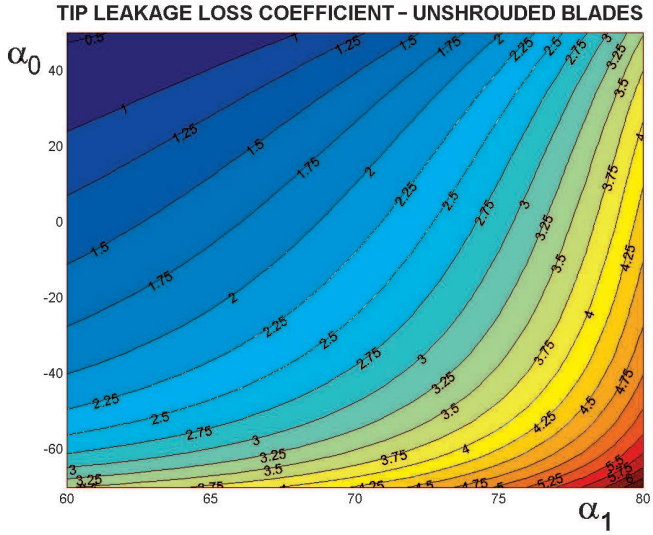

Figure 6. Tip leakage loss coefficient for unshrouded blades calculated from Equation (9) as a function of cascade inlet and exit angles α_0, α_1; $\delta = 0.01h$, $C_\delta = 0.4$

The presented results can be considered a first approximation of the phenomena that accompany the tip leakage flow. This approximation does not take into account the effects of compressibility, usually very important in the case of LP turbine stages with long unshrouded blades. Validation of the presented results on experimental data is not that easy since it is not easy to separate the tip leakage loss from other components of endwall loss. Also most of detailed experimental investigations do not take into account the effect of relative motion of the blade tips and endwalls. Anyway it can be shown that the presented theoretical results are in agreement with the experimental data. For example, in the case of a cascade investigated in [31] with the inlet angle -45°, exit angle 64°, without a relative motion, the measured loss coefficient is equal to 8.7% for the tip gap size of 2.1% (this coefficient was measured as a difference in the total loss for the tip gap cascade of that gap size and the cascade with no tip gap). For the given combination of cascade angles, the loss coefficient predicted from the diagram 6 is equal to 2.3% (for the 1% tip gap size). Multiplying this value by the tip gap size and changing the contraction coefficient from 0.4 to 0.7 (corresponding to the case of no relative motion of blade tips and endwall) one can obtain the value of 8.5% ($2.3\% \times 2.1 \times 0.7/0.4 = 8.5\%$), which falls very close to the measured value. For another cascade presented in [34] (inlet angle

32°, exit angle 76°), also without a relative motion, the difference in measured values of total loss coefficient (related to the inlet velocity) for two tip gap sizes of 2.8% and 1.7% (related this time to the profile chord) amounts to 7.5%. After recalculation of the loss coefficient into a value related to the exit velocity ($U_1 = 1.7U_0$) and making the tip gap size non-dimensional with respect to the channel height (for this cascade the blade height-to-chord ratio $h/C = 2.11$), it can be found that the measured tip leakage losses are equal to 4.9% for every 1% tip gap size (referred to the channel height). For the given combination of cascade angles, the diagram 6 gives a value of loss coefficient 2.7%. Changing the contraction coefficient from 0.4 to 0.7 yields finally 4.7%, which again is very close to the measured value. A similar comparison can be made for the cascade investigated in [18] (though the loss values are measured there in the section located a short distance downstream of the cascade trailing edge and require further recalculation to obtain mixed out values of the loss coefficient) as well as for the cascade presented in [26]. However, this comparison will not be documented here for the sake of brevity.

Increased possibilities of investigating turbine flow phenomena, including tip leakage flow can be attributed to numerical modelling and development of flow solvers based on the RANS approach. Using numerical methods enables *e.g.* tracing the formation of the tip leakage vortex, its interaction with the main flow, passage vortex and other vortical flows. For this paper, a series of computations were made with the help of a flow solver FlowER (3D RANS, perfect gas equation, k-ω SST turbulence model, finite volume method, upwind differencing, ENO scheme), [35–37]. The calculations converging to a steady-state were made in a one blade-to-blade passage of the stator and rotor cascades on an H-type grid refined near the blade walls and endwalls ($y^+ = 1-2$), leading and trailing edges of the blades. Typically, there are 12–16 grid cells in each boundary layer. The number of cells in one blade row reaches 500 000 (92 axially, 76 radially, 72 pitchwise). The calculation region extends also on the clearance over the rotor blades.

Numerical investigations were carried out on an impulse stage of an intermediate pressure (IP) turbine and a single rotor cascade of a high pressure (HP) turbine. The investigated IP stage has straight stator blades of height 100 mm with the standard profile N3 and straight unshrouded rotor blades with the profile R2. The characteristic dimensions of the stage cascades are: blade height-to-chord ratio $h/C = 0.97$ (stator) and 2.88 (rotor), pitch-to-chord ratio $p/C = 0.68$ (stator) and 0.79 (rotor). The exit-to-inlet pressure ratio is 0.70 (pressure drop from 4.3 to 3.0 bar), inlet temperature 152°C. The Mach number downstream of the stator is then 0.7, downstream of the rotor – 0.5. The investigations were made for a range of tip gap size from 1% to 3% of the channel height taking into account the relative motion between the blade tips and endwall. The investigated single HP rotor cascade has straight unshrouded blades of height 60 mm and profile R2. The basic geometric dimensions of the cascade are: blade height-to-chord ratio – 2.00, pitch-to-chord ratio – 0.75. The calculations of this cascade were made in a wide range of stagger angle, inlet angle and operating conditions typical for HP turbine stages changed by varying the exit pressure. The Mach number ranged between 0.2–0.6. These investigations were also made for different values of tip gap size, both with and without the effect of relative motion of the blade tips and endwall.

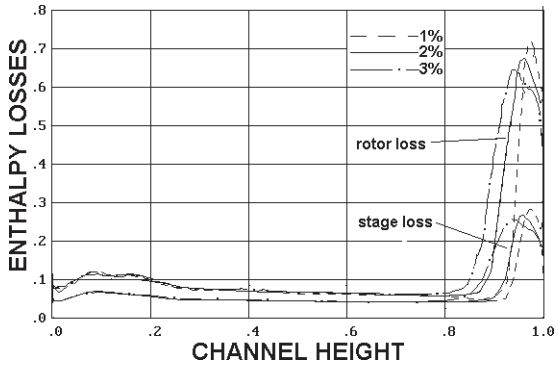

Figure 7. Spanwise distribution of enthalpy losses in the rotor and stage of an IP turbine calculated 40% axial chord downstream of the rotor trailing edge for three values of tip gap size

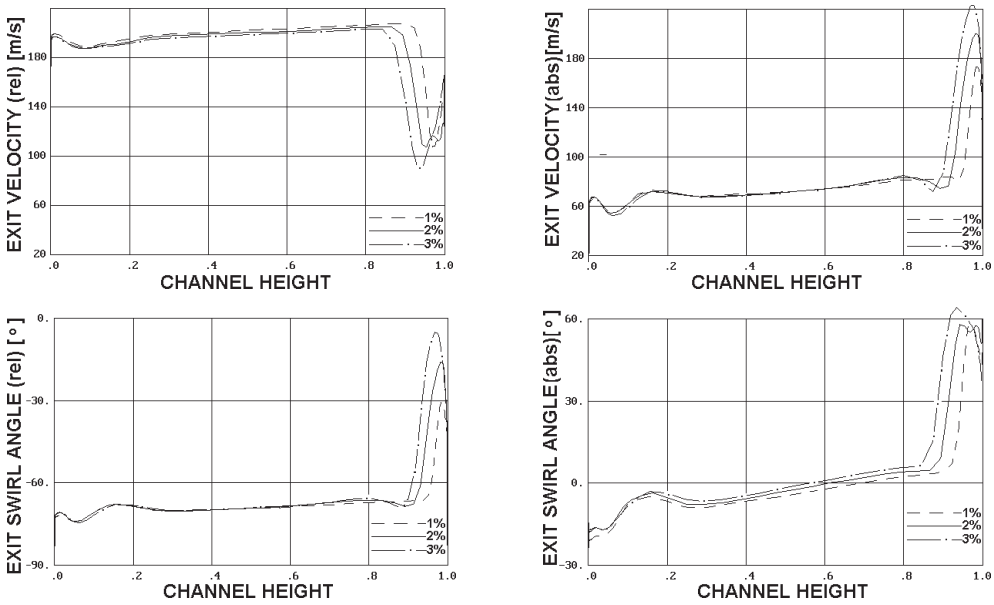

Figure 8. Spanwise distribution of exit velocity (top) and exit swirl angle (bottom) in the IP turbine stage in the rotating (left) and absolute (right) reference frame calculated 40% axial chord downstream of the rotor trailing edge for three values of tip gap size

Figure 7 illustrates spanwise distributions of enthalpy losses in the rotor and stage of the IP turbine calculated using the flow solver FlowER for three values of tip gap size at a section located 40% of the axial chord downstream of the rotor trailing edge. Expressions used to calculate stator, rotor and stage losses are enclosed in Appendix. The region of accumulation of the tip leakage loss is located near the tip endwall. The maximum value of the area distribution of loss falls within the tip leakage vortex and coincides with the place where the highest stresses occur. A typical spanwise distribution of loss contains a high peak near the tip endwall. Dissipation of this peak is usually not possible before the entry to the subsequent downstream stage. The tip leakage leads to non-uniformities in the spanwise distributions of the exit velocity and exit angle presented in Figure 8. These distributions were calculated in

the rotating and absolute reference frames also 40% of the axial chord downstream of the rotor trailing edge. In the rotating frame of reference, the velocity in the region of influence of the tip leakage vortex is typically lower than the velocity of the expanding main stream. In the absolute reference frame, the velocity in the tip leakage region is typically much larger than that of the main stream, exceeding it by over 100 m/s in the illustrated section. Since the leakage flow is deflected in another direction compared to the main flow, there is a large discrepancy between the exit swirl angle in the region of leakage and in the main stream. In the illustrated section, this discrepancy reaches 60°.

The form of the presented spanwise distributions depends on the location of the control section and evolves downstream as a result of dissipative processes taking place in the flow. The effect of tip leakage non-uniformities on the subsequent blade losses will be discussed later in this paper – in connection with leakage over shrouded blades in Section 7, over unshrouded blades in Section 8.

4. Effects of geometric and flow parameters on the tip leakage over unshrouded blades

4.1. Tip gap size

Figure 9 illustrates secondary flow vectors in a section located 25% of the axial chord downstream of the IP rotor trailing edge, which clearly exhibit the presence of two vortex structures – tip leakage vortex and passage vortex. The relation between the size of the tip leakage vortex and passage vortex depends on the tip gap size. In the investigated range of tip gap size the passage vortex remains closer to the tip endwall, whereas the centre of the tip leakage vortex is moved towards mid-span sections, its size considerably larger than that of the passage vortex. The total pressure contours at the trailing edge and downstream presented in Figure 10 also exhibit an increase in size of the tip leakage vortex and reduction in size of the tip passage vortex with the increasing tip gap size. The smaller intensity of the tip passage vortex as compared to that of the hub passage vortex can be due to the fact that part of the tip boundary layer is rolled up into the tip leakage vortex (for the case of a small gap size) and (for

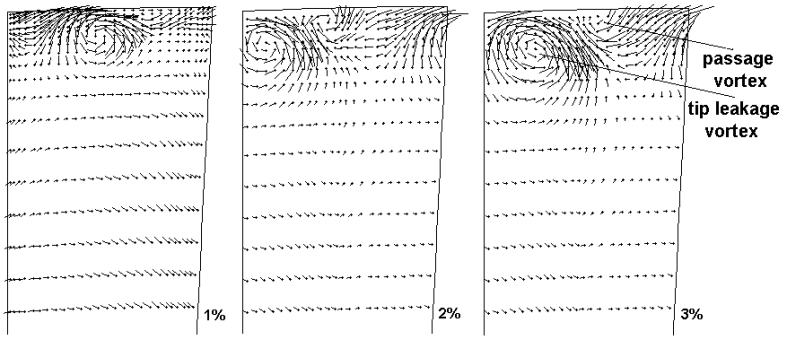

Figure 9. Secondary flow vectors in the IP rotor 25% axial chord downstream of the trailing edge for three values of tip gap size. Warning! Velocity vectors are not arrows but dots with a stretch showing the vector direction

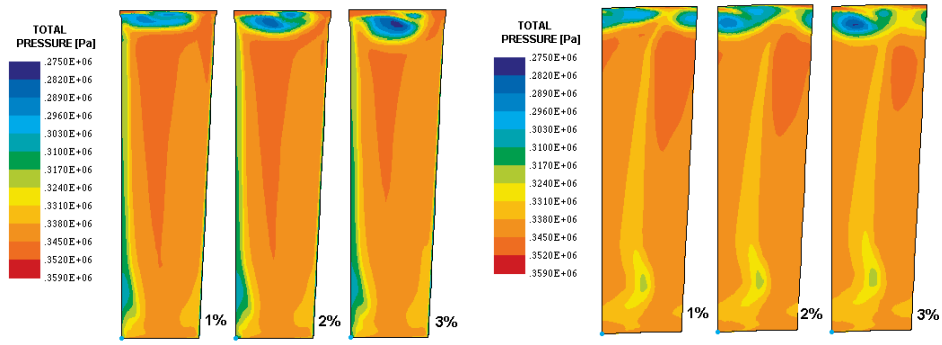

Figure 10. Total pressure contours in the IP rotor at the trailing edge section (left) and 25% axial chord downstream of the trailing edge (right) for three values of tip gap size

larger tip gaps) takes part in rotation with the endwall over the tip leakage flow (in a reference frame connected with the blade tip).

4.2. Flow turning in the cascade

Besides the tip gap size, the picture of interaction of the tip leakage vortex and passage vortex depends on the flow turning in the cascade. In the case of a relatively lower flow turning and lower load of an investigated HP cascade (profile stagger angle -13°, inlet angle 63°, exit angle -63°, $\mathrm{Ma} = 0.2$), a quick disintegration of the tip passage vortex as a result of interaction with a more intensive structure of the tip leakage vortex and the moving endwall is observed in Figure 11, showing secondary flow vectors and total pressure contours in subsequent sections upstream and downstream of the trailing edge. The passage vortex can be distinguished as a counter-rotating structure within the blade-to-blade passage, but it is already dissipated at the trailing edge and further downstream. In the exit section the largest losses appear top and right from the centre of the tip leakage vortex, that is in the region where the tip passage vortex was dissipated.

The interaction of the tip leakage vortex and passage vortex looks quite different in the case of a larger flow turning and larger load of the cascade (profile stagger angle -18°, inlet angle 75°, exit angle -72°, $\mathrm{Ma} = 0.4$) illustrated in Figure 12. In this case

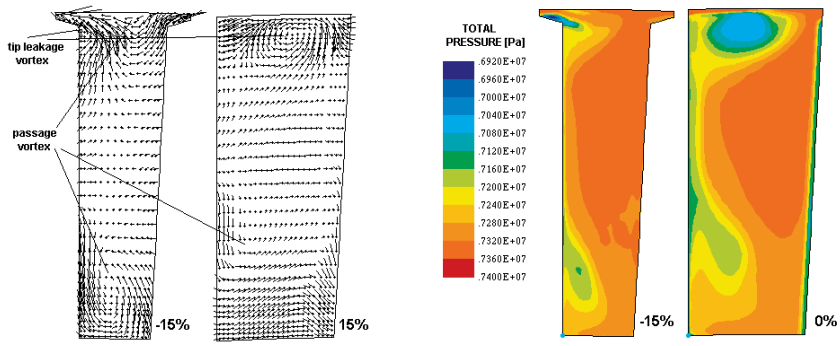

Figure 11. Secondary flow vectors and total pressure contours in the HP rotor cascade in selected sections located 15% axial chord upstream of the trailing edge, at the trailing edge and 15% axial chord downstream of it; tip gap size – 2%, $\mathrm{Ma} = 0.2$, $\alpha_0 = 63^{\circ}$, $\alpha_1 = -63^{\circ}$

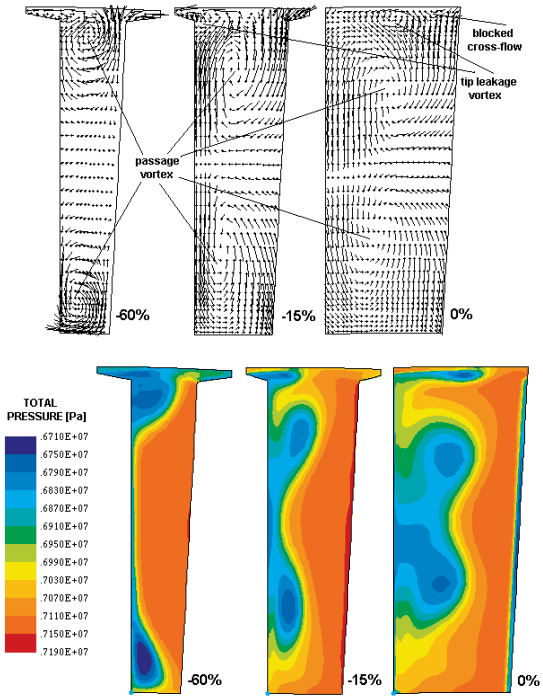

Figure 12. Secondary flow vectors and total pressure contours in the HP rotor cascade in selected sections located 60% and 15% axial chord upstream of the trailing edge and at the trailing edge; tip gap size – 2%, Ma = 0.4, $\alpha_0 = 75^\circ$, $\alpha_1 = -72^\circ$

the role of the cross-flow in the endwall region is increased. The passage vortex is formed before the tip leakage flow leaves the tip gap. The tip leakage pushes the passage vortex towards mid-span sections, rolls up into a tip leakage vortex blocking further cross-flow that is formed near the trailing edge. This cross-flow can possibly be rolled up again at the pressure surface above the tip leakage vortex. If this happens the new passage vortex is quickly dissipated by the interaction with the stronger tip leakage vortex.

4.3. Inlet angle

The comparison of total pressure contours at the trailing edge of the HP rotor cascade for the incidence angle changing between 44° and 74° is presented in Figure 13. The calculations were made taking into account the relative motion of the blade tips and endwall, assuming the constant static pressure drop across the cascade. There are some changes in the exit Mach number and exit angle from 0.15 and $\alpha_1 = -62.5^\circ$ for $\alpha_0 = 74^\circ$ to 0.2 and $\alpha_1 = -63.5^\circ$ for $\alpha_0 = 44^\circ$, respectively. Figure 13 shows that the area picture of tip leakage loss does not considerably alter with the changing incidence angle, whereas the size of the passage vortex at the opposite endwall depends very much on the incidence angle.

4.4. Relative motion of the blade tips and endwall

The relative motion of the blade tips and endwall takes an important part in the process of formation of tip leakage flow. This problem was scrutinised in [30, 34]; the

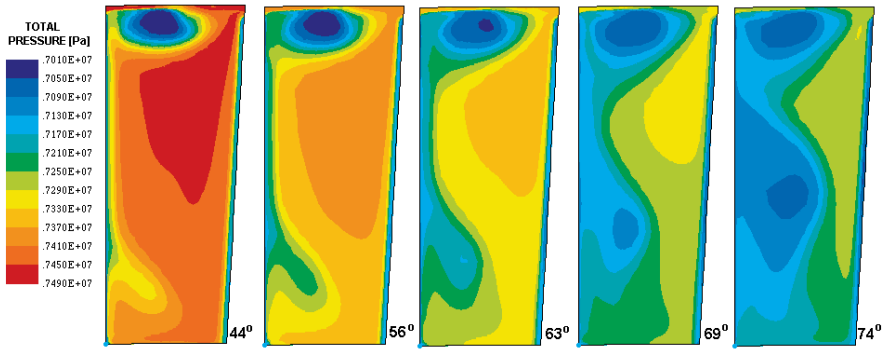

Figure 13. Total pressure contours in the HP rotor cascade at the trailing edge; tip gap size – 2%, $0.15 \leq \mathrm{Ma} \leq 0.2$, $-63.5^{\circ} \leq \alpha_1 \leq -62.5^{\circ}$

effect of rotating endwall in the range of rotational speed from 0 do 100% EES (engine equivalent speed) was investigated, where 100% EES corresponds to the nominal rotation velocity of the blade in the endwall section. The investigations show that the increase of the rotational speed decreases the mass flow rate of the tip leakage and the intensity of the tip leakage vortex. There are two mechanisms responsible for this tendency – first, due to the increased stresses between the leakage stream and the moving endwall rotating in the opposite direction, second, due to the increased static pressure at the exit from the tip gap, which leads to a reduction of the pressure drop across the tip gap.

The latter effect can be viewed in Figure 14 that illustrates the results of this author's investigations of static pressure in the mid-gap section of the HP rotor cascade (at 99% of the channel height) without the relative motion (when the endwall rotates together with the blades) and with the relative motion (when the blade rotates at its nominal speed and the endwall remains static) for 2% tip gap size. For reference, the static pressure contours in the blade-to-blade passage located 80% of the channel height from the hub are also shown in this picture. The region above the rear part of the blade is characterised by the decreased pressure quantitatively different from the pressure decrease at the suction surface in the blade-to-blade passage. The pressure drop across the tip gap in the case of relative motion is by more than 20% larger than in the case of no relative motion of the blade tips and endwall.

The case of no relative motion does not have a practical meaning, however investigations of this case are important from the cognitive point of view. They enable realisation of the fact that the relative motion is a factor that causes considerable reduction of the tip leakage losses. Figure 15 illustrates the comparison of total pressure contours upstream and at the trailing edge of the investigated HP rotor cascade calculated without and with the relative motion. The relative motion decreases the flow rate through the tip gap. Both vortex structures (tip leakage vortex and tip passage vortex) are pushed towards the suction surface of the blade tip. The exit from the tip gap is partly blocked by the intensified cross-flow leading to the increased static pressure at the tip gap exit. As a final effect, the intensity of the tip leakage vortex is significantly reduced. The effect of endwall rotation on the passage vortex is not that clear. The intensified cross-flow may appear first at the suction surface of the blade

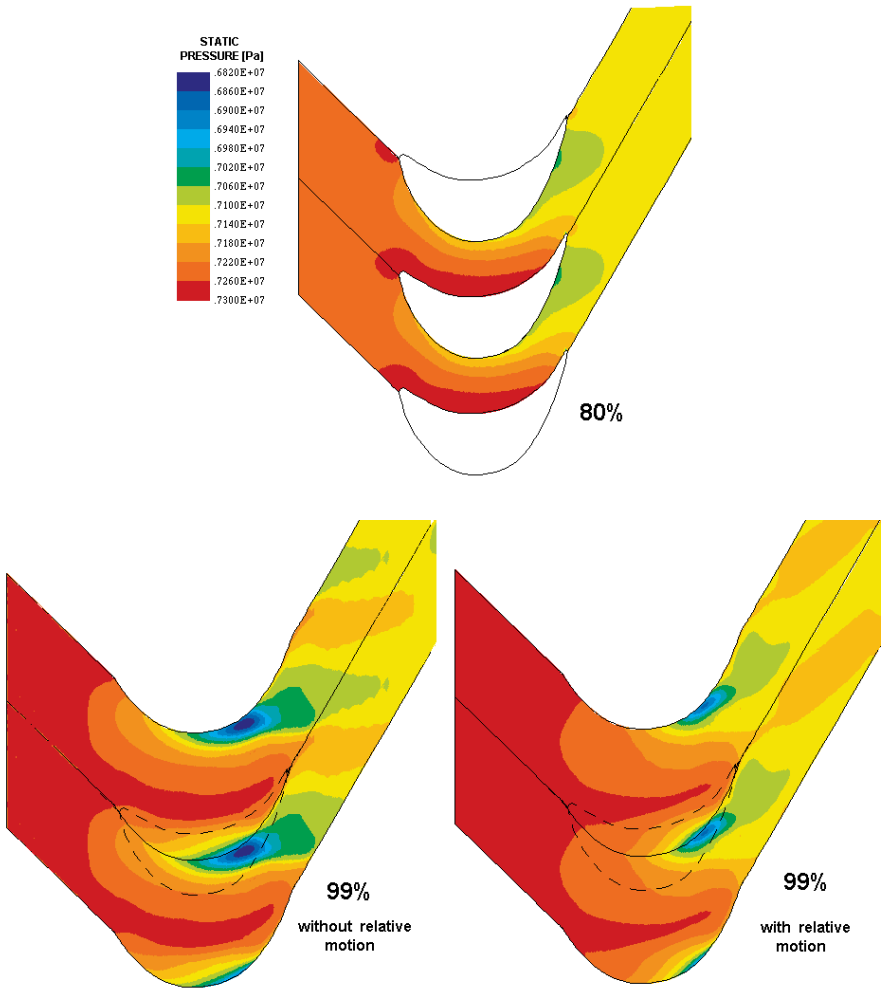

Figure 14. Static pressure field in the blade-to-blade passage located 80% channel height from the hub (top) and in the mid-gap section of the HP rotor cascade calculated without relative motion (bottom-left) and with relative motion (bottom-right); tip gap size – 2%

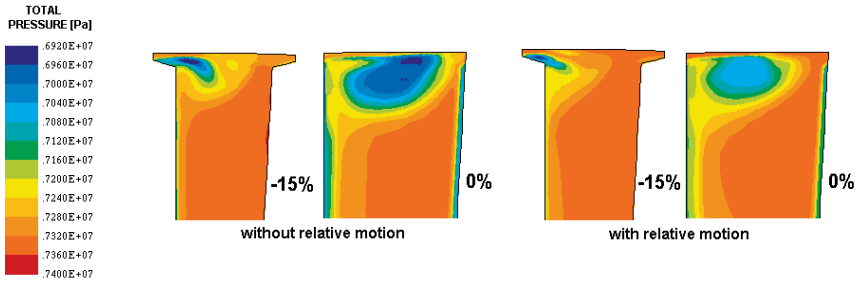

Figure 15. Total pressure contours 15% axial chord upstream of the trailing edge and at the trailing edge of the HP rotor cascade calculated without relative motion (left) and with relative motion (right); tip gap size – 2%

and roll up there before the tip leakage vortex is formed. Traces of this roll-up can be found at the suction surface below the passage vortex. On the other hand, a smaller area occupied by the passage vortex top and right from the tip leakage vortex may be due to the fact that at a sufficient tip gap size much of the cross-flow does not roll-up into the structure of the passage vortex and takes part in rotation with the endwall over the tip leakage. It follows from [26] that the relative motion of the blade tips and endwalls typically leads to a decrease of the tip leakage losses even by as much as a half, as compared to the case of no relative motion.

5. Formation of leakage over shrouded rotor blades

The driving force of the leakage flow over shrouded rotor blades is the pressure difference in the blade-to-blade passage between the leading and trailing edges of the blades. In the case of reaction turbine stages this difference is typically comparable to the mean pressure difference between the pressure and suction side of the blade. In the case of impulse stages, the pressure difference between the leading and trailing edge is much lower. The geometry of the region where the leakage over shrouded blades is formed is usually more complex than that of the tip leakage over unshrouded blades and assumes the shape of a labyrinth. A simplified model of leakage flow over the shroud with a single seal that can be used for the purpose of estimation of leakage loss, [3], is presented in Figure 16. The model picture of the leakage is in some sense similar to that of the tip leakage over unshrouded blades. The leakage flow forms a narrow stream between the seal and endwall. The leakage stream separates from sharp edges of the shroud and seals, which is accompanied by formation of recirculation zones in labyrinth seal chambers. At the exit from the labyrinth the leakage stream is subject to mixing with the main stream in the blade-to-blade passage. This process takes place downstream of the blade trailing edges, usually under positive pressure gradient conditions. Thus, unlike in the case of tip leakage over unshrouded blades, the leakage flow over the shroud does not roll-up into a vortex structure but forms an axisymmetric (in first approximation) mixing zone.

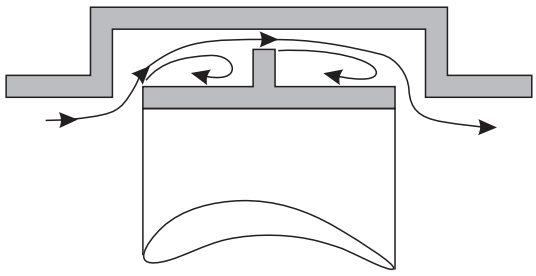

Figure 16. Scheme of the leakage flow over shrouded turbine blades with a one-seal labyrinth, [3]

The pressure difference between the inlet and exit section of the labyrinth seal as well as its geometry are the main factors that determine the mass flow rate of the leakage flow. The leakage stream experiences some entropy rise on its way through the labyrinth due to friction against the endwall, shroud and seal elements and due to mixing of the leakage stream with vortex layers separating it from the

recirculation zones. On the re-entry to the blade-to-blade passage the leakage stream carries high-energy fluid and is characterised by parameters different than those of the main flow, giving rise to mixing of the streams. Typically, most of entropy creation due to leakage flow takes place not in the labyrinth seal region but in the blade-to-blade passage downstream of the leakage jet re-entry slot, [3].

6. Leakage loss diagram for shrouded blades

The main loss mechanisms in the region of leakage flow over the shroud are in major part analogical to those of the tip leakage over unshrouded rotor blades. They are:

1. friction of the leakage stream against the endwall, shroud and labyrinth seal elements;
2. shear effects within the labyrinth seals in the non-uniform leakage stream and in the recirculation zones (especially at the borders of recirculation zones);
3. dissipation of secondary kinetic energy of the leakage stream during its mixing with the main flow downstream of the rotor blade trailing edges. The entire secondary kinetic energy of the leakage stream with respect to the main stream can be assumed lost during this mixing process;
4. reduction of the tip secondary flows caused by the outflow of the low-energy boundary layer fluid into the leakage slot;
5. at a close distance to the next stage stator blade, the mixing processes due to the leakage stream are hardly accomplished in the current blade row and are continued in the subsequent stator. The main source of subsequent blade losses are non-nominal inflow conditions resulting from the discrepancy between the velocity directions of the leakage and main stream.

Assuming that the leakage flow in the labyrinth seal is subject to a pressure drop analogical to that of the main stream in the blade-to-blade passage, that is from p_1 to p_2, the leakage losses in the labyrinth region over the shroud can be determined using a simplified enthalpy-entropy (h-s) diagram presented in Figure 17, either in terms of entropy rise due to dissipative processes taking place in the labyrinth chamber, that is $s_{2'} - s_1$, or in terms of lost part of the theoretical enthalpy drop corresponding to

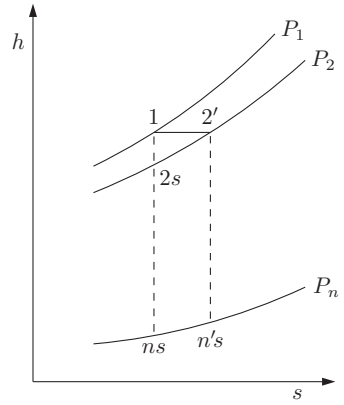

Figure 17. Diagram of expansion of the leakage flow over shrouded blades

the isentropic expansion conditions, that is $h_{n's} - h_{ns}$. Leakage losses in the region over the shroud are often referred to as "by-pass" losses, *e.g.* [38]. At the exit from the labyrinth seals the leakage stream is theoretically capable of performing work in the subsequent stage. However, it is also subject to mixing with the main stream.

Mixing losses in the blade-to-blade passage due to leakage over shrouded rotor blades can be estimated from the model of lost kinetic energy of the leakage stream relative to that of the main stream. It is assumed in [3] that the mixing takes place at the downstream pressure in the blade-to-blade passage p_1, that is $p_j = p_1$, and that there is no total pressure loss in the main stream nor in the leakage stream on its way through the labyrinth seal, that is $p_{jT} = p_{0T} = p_{1T}$. Assuming that the swirl velocity of the leakage stream does not change through the labyrinth seal and remains the same as the main stream velocity at the entrance to the rotor, the total pressure balance for a labyrinth seal section (the Bernoulli equation) yields:

$$\frac{1}{2}\rho\left(V_{jx}^2 + V_x^2 \operatorname{tg}^2\alpha_0\right) + p_j = \frac{1}{2}\rho\left(V_x^2 + V_x^2 \operatorname{tg}^2\alpha_0\right) + p_0, \tag{11}$$

where V_{jx} denotes the axial component of the leakage stream in the labyrinth, V_x is the axial component of the main stream velocity, $V_x \operatorname{tg}\alpha$ is the swirl velocity in the blade-to-blade passage (the radial velocity is assumed equal to zero). From the equality $p_{0T} = p_{1T}$ one can obtain:

$$\frac{1}{2}\rho\left(V_x^2 + V_x^2 \operatorname{tg}^2\alpha_0\right) + p_0 = \frac{1}{2}\rho\left(V_x^2 + V_x^2 \operatorname{tg}^2\alpha_1\right) + p_1. \tag{12}$$

Making use of the assumption that $p_j = p_1$ gives:

$$V_{jx}^2 = V_x^2\left(1 + \operatorname{tg}^2\alpha_1 - \operatorname{tg}^2\alpha_0\right), \tag{13}$$

from which the mass flow of the leakage stream can be found as:

$$m_j = \rho C_\delta \delta p V_x \sqrt{1 + \operatorname{tg}^2\alpha_1 - \operatorname{tg}^2\alpha_0}, \tag{14}$$

where δ is the clearance above the shroud, C_δ denotes the contraction coefficient for a single-seal geometry, which remains a function of the sealing geometry. In the present calculations the value of the contraction coefficient is assumed the same as for the case of unshrouded blades, that is 0.4, and the main stream mass flow rate is defined by Equation (4). Assuming that at the exit from the labyrinth the leakage jet loses its axial velocity and turns radial into the blade-to-blade passage, its components can be defined as:

$$\mathbf{V}_j = [0,\, V_x \operatorname{tg}\alpha_0,\, -V_{jx}]. \tag{15}$$

The velocity of the main flow can be written as:

$$\mathbf{V}_1 = [V_x,\, V_x \operatorname{tg}\alpha_1,\, 0]. \tag{16}$$

Thus the loss coefficient due to mixing of the leakage flow with the main stream calculated from the condition of lost relative kinetic energy of the leakage can be found in the form ($m_j \ll m_1$), [3]:

$$\begin{aligned}\xi &= \frac{m_j}{m_2}\frac{e_{rel}}{e_2} = \frac{m_j}{m_2}\frac{V_{rel}^2}{V_2^2} \approx \frac{m_j}{m_1}\frac{V_{rel}^2}{V_1^2} = \frac{m_j}{m_1}\frac{V_x^2 + V_x^2\left(\operatorname{tg}\alpha_1 - \operatorname{tg}\alpha_0\right)^2 + V_{jx}^2}{V_x^2 + V_x^2 \operatorname{tg}^2\alpha_1} \\ &= 2\frac{m_j}{m_1}\left(1 - \frac{\operatorname{tg}\alpha_0}{\operatorname{tg}\alpha_1} sin^2\alpha_1\right).\end{aligned} \tag{17}$$

Changes of the shroud leakage loss coefficient calculated from Equation (17) as a function of cascade inlet and exit angles α_0, α_1 for a 1% clearance assuming that $C_\delta = 0.4$ are illustrated in Figure 18. Flow losses due to the leakage over shrouded blades change in a wide range depending on the combination of inlet and exit angles. For typical inlet/exit angles of reaction cascades the leakage loss coefficient for shrouded blades is comparable with that of unshrouded blades (at the same effective clearance δC_δ). More significant differences are for combinations of inlet/exit angles typical for impulse cascades. For $\alpha_0 = (-65^\circ, -60^\circ)$, $\alpha_1 = (65^\circ, 75^\circ)$, the loss coefficient varies between 1.5–4.0% for every 1% clearance and is lower than for the case of unshrouded blades. It is assumed that these results remain valid for a single-seal configuration. Increasing the number of seals leads to a reduction of the leakage stream flow rate, which refers both to the reaction and impulse cascades. For a labyrinth configuration with several seals, the loss coefficient can be calculated from Equation (17) assuming the effective clearance size as $C_\delta \delta/\sqrt{N}$ (N – number of seals), which means that for 4 seals the loss coefficient is reduced twice compared to the case of a single seal. Detailed empirical correlations to determine the intensity of leakage flows and the resulting flow losses for different types of labyrinth seals can be found *e.g.* in [39]. The relation (17) should be considered approximate. In HP turbine stages with short-height blading particularly important is interaction of the leakage stream with secondary flows of the current and subsequent blade row, as shown in [40–42].

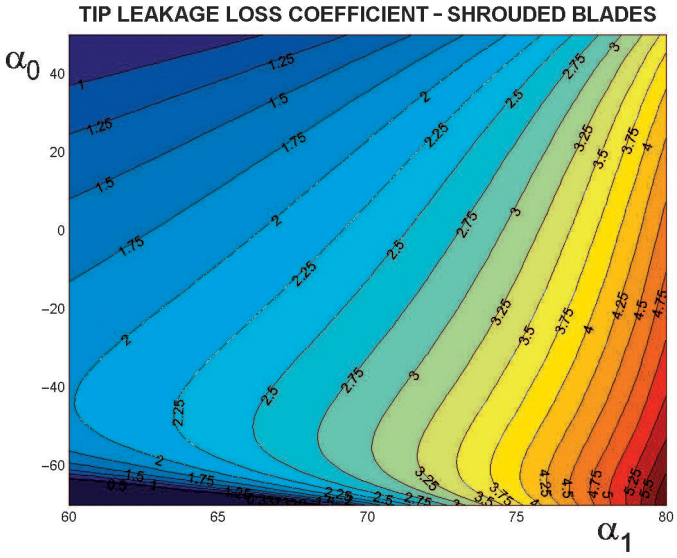

Figure 18. Leakage loss coefficient for shrouded blades calculated from Equation (17) as a function of cascade inlet and exit angles α_0, α_1; $\delta = 0.01h$, $C_\delta = 0.4$

7. Leakage/main flow interactions

In this section the interaction of leakage flows with the main stream is investigated numerically with the help of flow solver FlowER. In addition to the boundary conditions typical for turbomachinery codes, source/sink-type boundary

conditions are used at places at the endwalls referring to design locations of injection of leakage and windage flows into, or their extraction from, the blade-to-blade passage, see Figure 19. For extractions (sinks), one boundary condition is needed – mass flow rate. For injections (sources), there are four boundary conditions – mass flow rate, total temperature, meridional and swirl angle. The source/sink gaps belong to the rotor domain, so the source/sink terms are resolved in the rotating reference frame. The mass flow rate condition is formulated to be satisfied integrally through each slot, and is allowed to vary from node to node of the slot. The distribution of mass flow rate in the slot is affected by the stream-wise and pitch-wise gradients of static pressure in the rotor near the endwalls. The velocity components at the source slot are calculated based on the constant total pressure, input flow angles and size of the slot. The presented method enables computation of interaction of the leakage flows with the main stream, secondary flows, separations and other phenomena, [40].

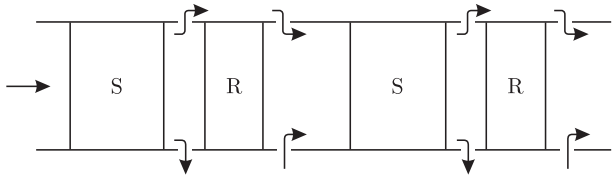

Figure 19. Computational domain with source/sink-type permeable boundaries to simulate the effect of leakage over the shroud and windage flows in impulse turbines; S – stator, R – rotor

The computed group of two HP impulse stages comes from a 200 MW steam turbine. The short-height straight blades have profiles of type PŁK (stators) and R2 (rotors). The characteristic stage dimensions are: span/chord – 0.75 (stators) and 2.0 (rotors), pitch/chord – 0.75 (stators and rotors), span/diameter – 0.08. The stage group operates at the pressure drop from 88 to 70 bar, inlet temperature – 760K, flow rate – 170 kg/s, average stage reaction – 0.15. Prior to CFD computations, the stage group was scrutinised with the aid of a 1D code TUR-96 [43, 44] to evaluate the mass flow rate of the main flow in the blade-to-blade passage of the stator and rotor G_1, G_2 as well as the mass flow rates of the tip and root leakages G_T, G_R, and windage flows G_W, $G_{W'}$ based on the given pressure drops and geometry of labyrinth seals and passages. The results obtained from the 1D approach necessary for further 3D computations are as follows: $G_T = 2.7\%G_1$, $G_W = G_{W'} = 1.2\%G_1$.

First, 3D RANS computations were made for a single turbine stage making use of the Baldwin-Lomax turbulence model in three variants: (1) without side flows with source/sink slots closed, (2) with only tip leakage slots open, (3) with both tip leakage and windage flow slots open. In source/sink computations, it was assumed by way of example that the fluid is injected through the source slots in the radial direction (no axial and swirl velocity). These investigations, in parallel with the problem of leakage over shrouded blades, also treat the problem of windage flows that can have a consequence for flow efficiency at the hub sections in the blade-to-blade passage. Windage flow losses are boundary layer losses at stationary and rotating discs as well as mixing losses in the blade-to-blade passage after returning of the windage flow to the main flow. The loss of power due to friction of the medium against the disc surface was evaluated in [3]. Typically its value is a negligible component of the

overall loss. It can be expected that the mixing losses of the windage flow returning to the blade-to-blade passages with the main flow form a more contributing loss factor. Typically, mixing losses due to windage flows are 2–5 times lower than those of the leakage over the shroud.

Second, 3D RANS computations were made for the two-stage group with the help of the Menter k-ω SST turbulence model, taking into account only the leakage flow over the shrouded blades, with hub leakages neglected. In these investigations, the swirl angle of the tip leakage jet was assumed equal to 80°, which corresponds to the swirl angle of the main flow downstream of the stator cascade (measured clockwise from the projection of the turbine axis in the blade-to-blade plane). The meridional angle of the tip leakage jet was assumed –90° (measured clockwise of the turbine axis in the meridional plane, meaning no axial velocity at the re-entry to the blade-to-blade passage). Also in order to determine the effect of leakage mass flow rate and leakage jet direction at the re-entry to the blade-to-blade passage on the flow efficiency, additional investigations were carried out where the tip leakage mass flow rate was varied from 1% up to 4% of the flow rate in the stator cascade, the swirl angle of the leakage jet at the re-entry varied from 0° to 80°, the meridional angle of the tip leakage jet changed from $-90°$ to $-30°$.

Leakage flows (both at the tip and root) leaving the main flow region help to remove the boundary layer fluid from the blade-to-blade passage upstream of the rotor into the leakage slot, which retards the development of secondary flows. This effect can be observed from the comparison of velocity vectors at the blade suction surface of the first rotor for the three investigated variants of flow presented in Figure 20. Sucking out the high-entropy boundary-layer fluid into the sink slot prior to the rotor brings a considerable reduction in the span-wise extension of the secondary flow zone and reduction of secondary flow losses as compared to non-source/sink computations. This is particularly clear at the tip endwall, perhaps less clear at the root sections, where an interference of the secondary flow zone with a separation zone is observed.

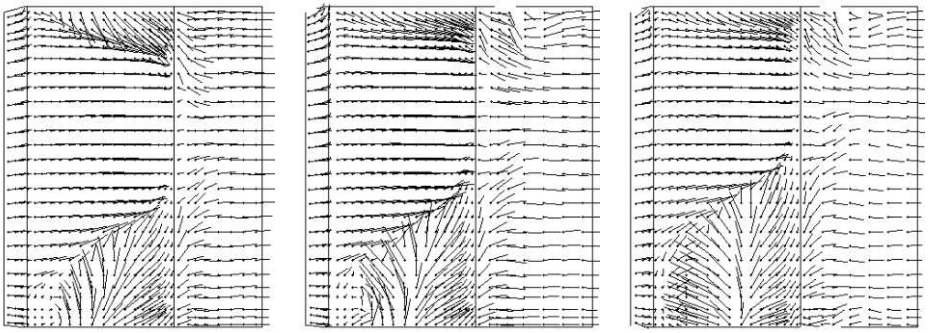

Figure 20. Velocity vectors in the rotor at the suction surface – computed without sources and sinks (left), computed with tip leakage (centre), computed with tip leakage and windage flows (right)

On the other hand, leakage flows act as a mass deficit for the blade-to-blade passage. The mean axial velocity is reduced, which may locally increase the incidence angle. This effect can be observed in Figure 21 showing entropy function contours and

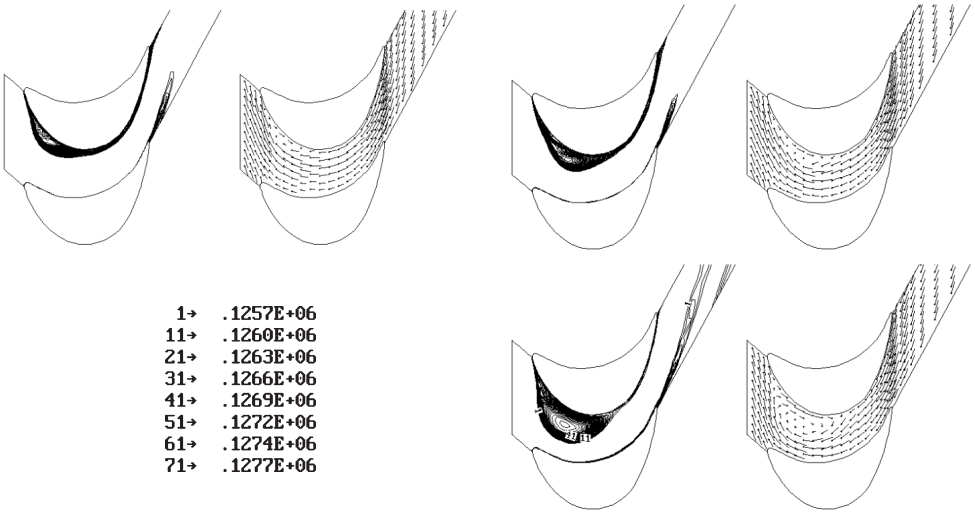

Figure 21. Entropy function contours and velocity vectors in the rotor at 9% blade span from the root – computed without sources and sinks (top-left), computed with tip leakage (top-right), computed with tip leakage and windage flows (bottom)

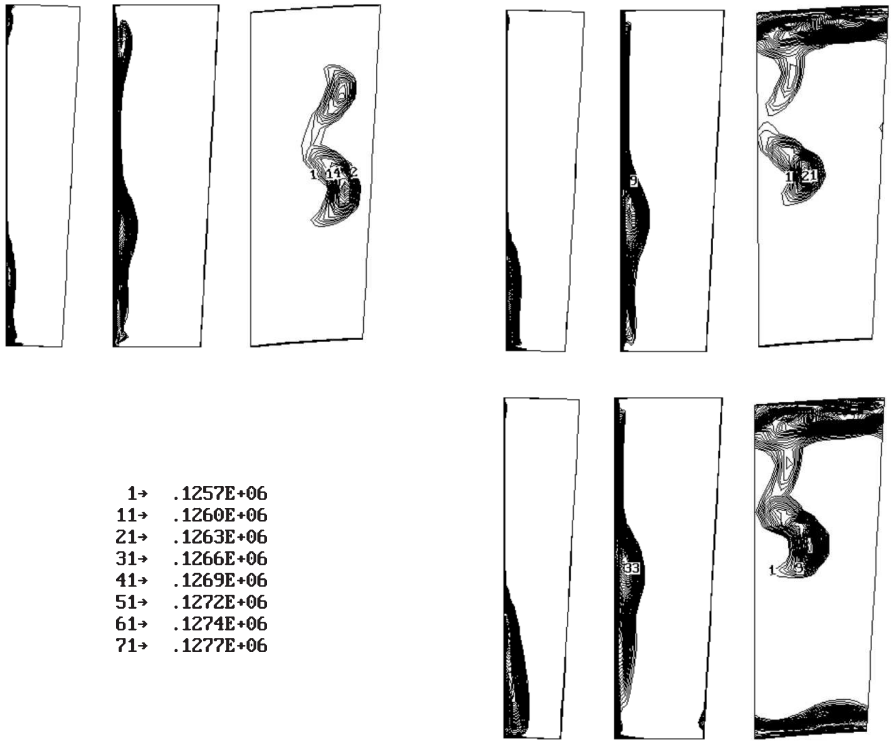

Figure 22. Entropy function contours in the rotor 50% axial chord from the leading edge, at the trailing edge and 45% axial chord from the trailing edge – computed without sources and sinks (top-left), computed with tip leakage (top-right), computed with tip leakage and windage flows (bottom)

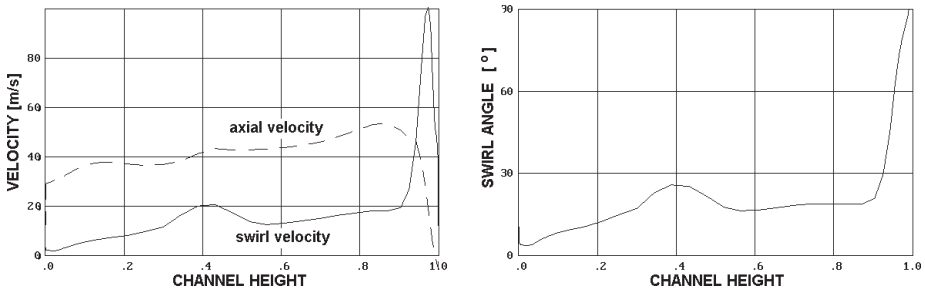

Figure 23. Span-wise distribution of axial and circumferential velocities (left) and swirl angle (right) at the inlet to stage 2

velocity vectors in the first rotor in a section located 9% of the blade height from the hub for the three investigated variants of flow. Due to the increased incidence at the rotor in computations taking into account leakage effects, the size of the separation zone that occurs up to 35–40% of the blade span from the hub increases, as compared to non-source/sink computations. This also refers to the situation where only tip leakage flow is considered, which means that the effect of tip leakage flow does not only have a local character restricted to the tip region, but it can also change flow patterns at the opposite endwall. Further outflow of the medium into the windage flow slot further increases the size of the separation zone and separation losses, which can also be observed from the entropy function contours in subsequent sections of the rotor (inside the blade-to-blade passage, at the trailing edge and downstream in the wake) illustrated in Figure 22. Downstream of the leakage jet re-entry, source/sink computations exhibit the zones of mixing of the leakage streams with the main flow, where major part of leakage losses is concentrated.

Similar to the case of leakage over unshrouded rotor blades, leakage over the shroud leads to non-uniformity in the exit velocity as shown in Figure 23. Downstream of the rotor in the region of influence of the tip leakage typically reaching 10% of the blade height from the tip a reduction of the axial velocity and increase of the circumferential velocity and swirl angle in the absolute reference frame is observed. In the section located 45% of the axial chord from the rotor trailing edge, the axial velocity in the leakage region is lower by 50 m/s than in the main flow region, the swirl velocity is higher by 80 m/s, swirl angle higher by 60°. In contrary to the vortex structure of the leakage over free-tip blades, the leakage over the shroud is more uniform along the circumference. This feature can be observed in Figure 24 showing the comparison of total pressure contours in the axial gap between stages 1 and 2 of the IP turbine with unshrouded blades and HP turbine with shrouded blades. This figure is also thought to be an illustration of consequences of circumferential averaging of flow parameters in the assumed computational method (where only non-uniformities in the axial direction can be transmitted between the blade rows). The figure shows the area distribution of total pressure in the rotating reference frame of the rotor domain (at a section located 40% of the gap width) as well as after the averaging and transformation to the non-rotating reference frame of the next stage stator (at 90% gap width). It follows from the comparison that the effect of this averaging technique on the flow in the downstream stage is less important for the case of leakage over the

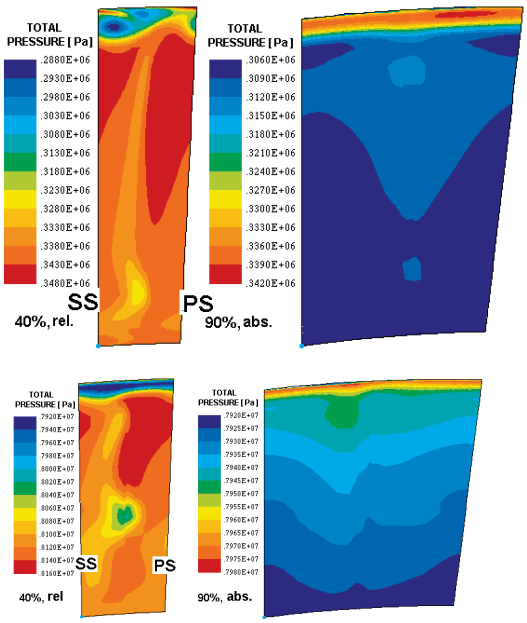

Figure 24. Total pressure contours in the axial gap between stages 1 and 2 of the IP turbine with unshrouded blades (top) and HP turbine with shrouded blades (bottom) in the relative frame of the upstream rotor at 40% axial gap width and after pitch averaging in the absolute frame of the downstream stator at 90% gap width

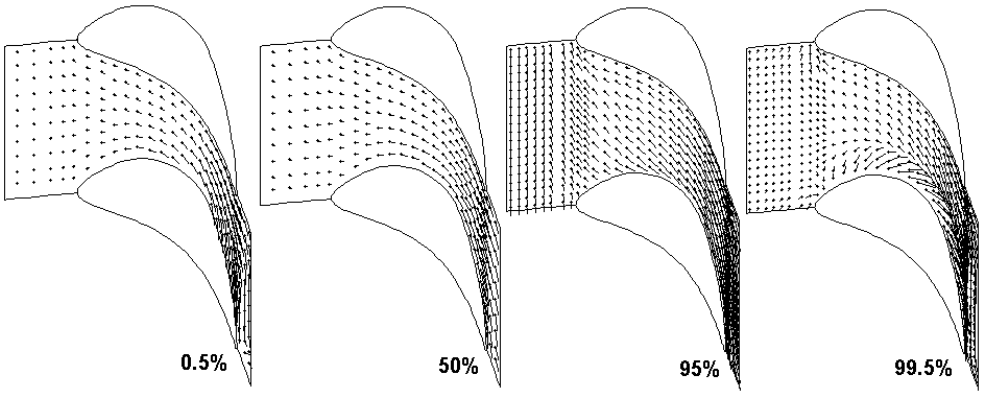

Figure 25. Velocity vectors in the second stator at the hub at 0.5% blade height, at the mid-span and in the tip leakage region 5% and 0.5% blade height from the tip

shroud. Therefore, this technique can be used to investigate downstream effects of the tip leakage over the shroud, whereas in the case of leakage over free-tip blades fully unsteady technique with exact transmission of flow parameters between the stators and rotors needs to be employed. It is also important to note here that the tip leakage region at the inlet to the next stator is a zone of high total pressure (in the absolute reference frame).

Figure 25 illustrates velocity vectors in the second stator in different blade-to-blade sections along the span. In the tip leakage region the incidence at the blade

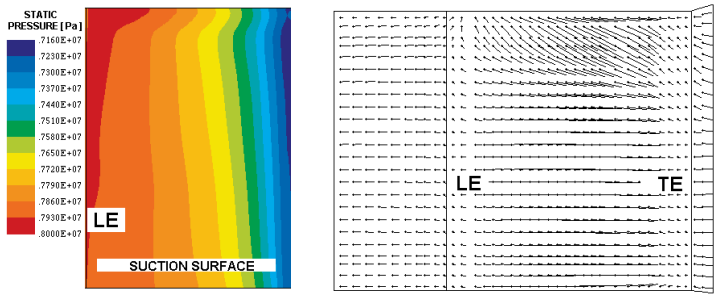

Figure 26. Static pressure contours and velocity vectors at the suction surface of the stator blade in the second stator; LE – leading edge, TE – trailing edge

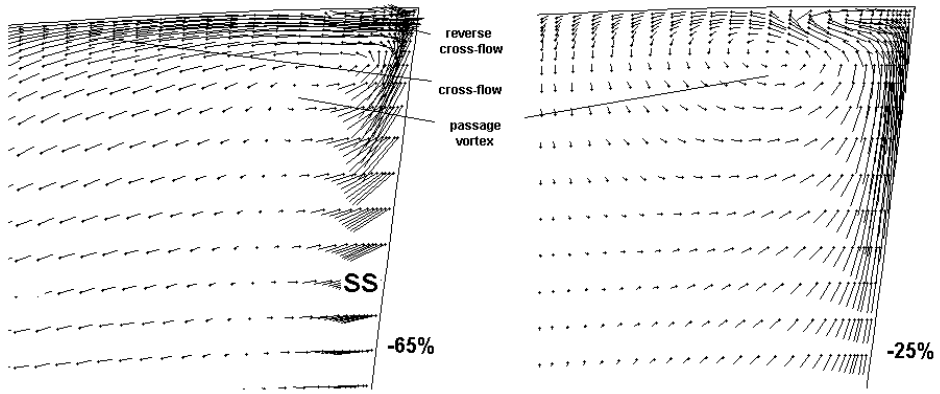

Figure 27. Secondary flow vectors in the second stator 65% and 25% axial chord upstream of the trailing edge; SS – suction surface

moves onto the suction surface where the stagnation point is situated. Besides the typical cross-flow from the pressure to the suction surface intensified by the non-nominal incidence, a reverse cross-flow from the suction surface is also observed at the front part of the blade, pushing the suction side leg of the horseshoe vortex away from the suction surface. Due to the relocation of the stagnation point in the tip leakage region, another important factor that defines the flow patterns are strong span-wise pressure gradients at the blade surfaces in the tip endwall region. Figure 26 illustrates static pressure contours and velocity vectors at the suction surface of the second stator blade. The downward pressure gradient at the suction surface in front part of the passage induces the motion of fluid elements in this direction. The opposite pressure gradient towards the tip endwall can be found at the pressure surface, giving rise to a strong recirculating flow, being a source of a large passage vortex that can be observed in Figure 27, showing secondary flow vectors in subsequent sections of the second stator. This recirculating flow induced by the local pressure gradients is much more intensive than that at the hub endwall and contains not only the boundary layer fluid but also the tip leakage fluid. Thus, the high-energy mixing zone of tip leakage flow is rolled up together with the endwall boundary layer into a strong structure of the passage vortex. Downstream the centre of the passage vortex moves towards the mid-span sections. In front part of the blade-to-blade passage, a thin layer of blocked

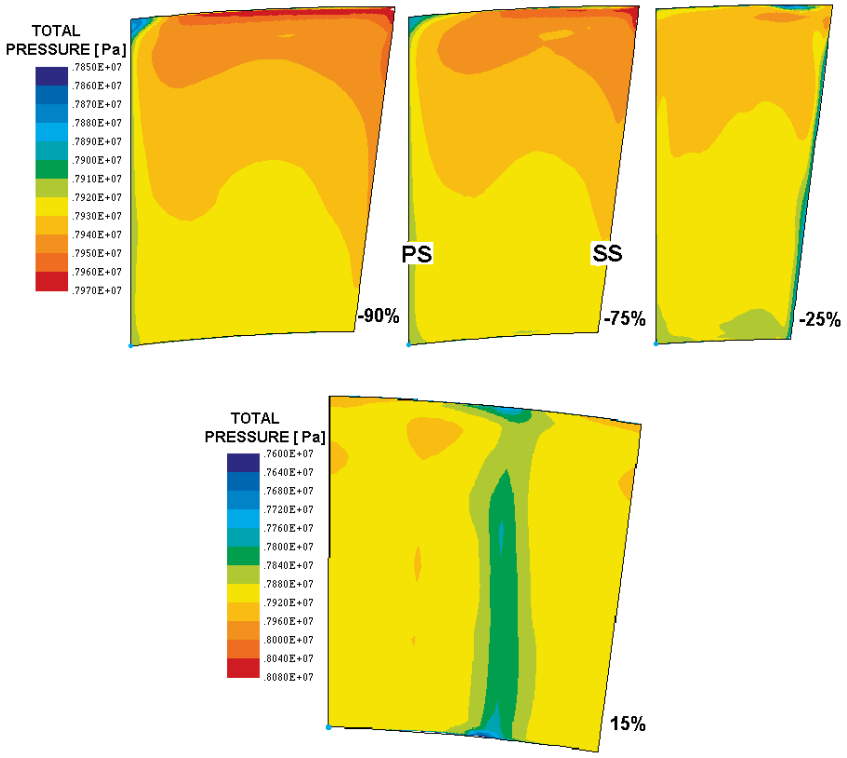

Figure 28. Total pressure contours in the second stator in subsequent sections located 90%, 75% and 25% axial chord upstream of the trailing edge and 15% axial chord downstream of the trailing edge

reverse cross-flow is observed in the endwall/suction surface corner, being a source of vorticity of the sense of rotation opposite to that of the passage vortex. Downstream, this corner is filled with a corner vortex coming from separation of the main passage vortex from the tip endwall.

The development of area loss distribution in the second stator can be observed in Figures 28 and 29 showing the total pressure contours and entropy function in the second stator in subsequent sections between the leading and trailing edge and further downstream. Figure 28 illustrates the process of a gradual decrease of the total pressure in the leakage-dominated region along the second stator passage surplus. Although the highest total pressure in the exit section is still observed in the upper part of the channel, most of the total pressure surplus is lost in the second stator. The loss centre due to the tip leakage from the upstream rotor moves together with the recirculating flow towards the suction surface and deep towards mid-span sections, Figure 29. Distinct places of the decreased total pressure and increased entropy function at the tip endwall corners are: at the front part of the pressure surface – the region of separation due to the non-nominal incidence, and near the suction surface – the region of blocked reverse cross-flow followed by the corner vortex from the separation of the recirculating main flow. For a comparison, Figure 29 shows also a picture of entropy function downstream of the second stator trailing edge calculated without taking into account the effect of tip leakage. As shown in Figure 30 illustrating

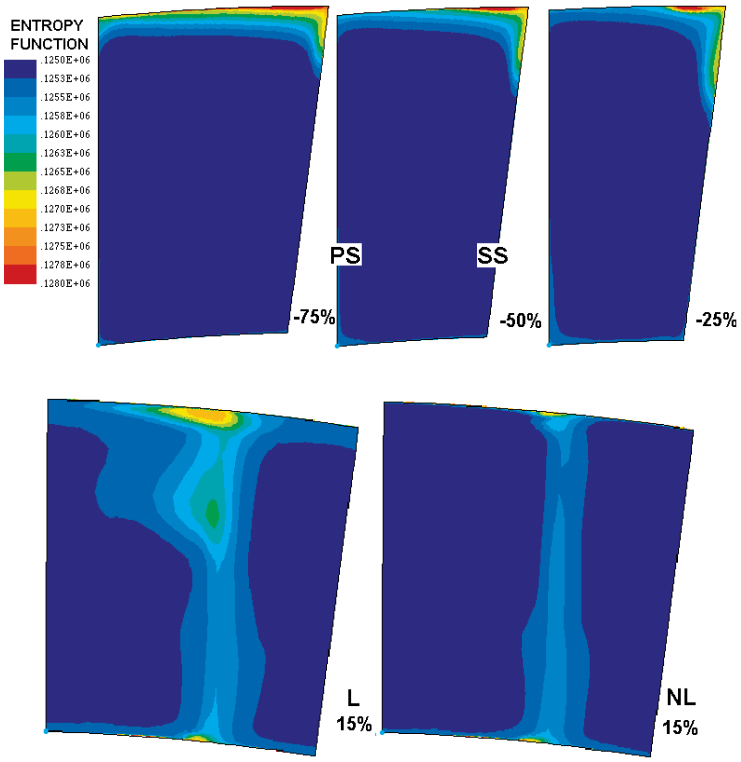

Figure 29. Entropy function contours in the second stator in subsequent sections located 75%, 50% and 25% axial chord upstream of the trailing edge (L). Also entropy function contours behind the second stator computed without leakage (NL)

the span-wise distribution of the exit swirl angle downstream of stator 1 and 2, the non-uniformities at the exit from the second stator increase to above 3°, which turns into 6–7° non-uniformities at the inlet to the second rotor after transformation to the rotating reference frame. It is worthwhile to note that the increase in size and intensity of the tip passage vortex in the next stator due to the influence of the tip leakage flow was also observed in experimental works [45, 43].

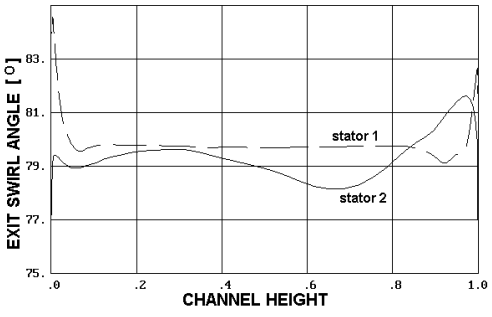

Figure 30. Span-wise distribution of the exit swirl angle downstream of stators 1 and 2; calculated with the leakage over the shroud

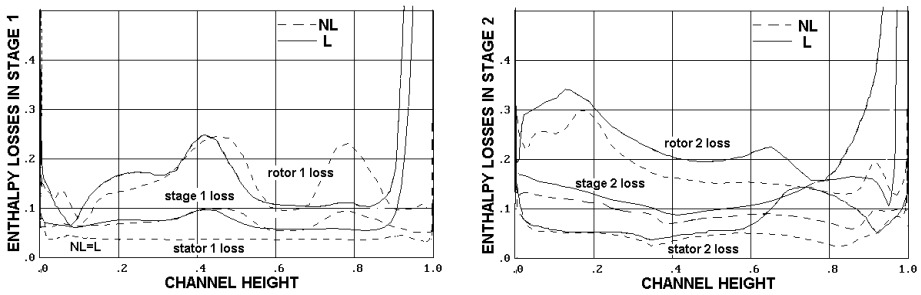

Figure 31. Stage 1 and 2: Span-wise distribution of enthalpy losses in the stator, rotor and stage; computed without (NL) and with tip leakage (L)

Table 1. Loss increase in the HP stage group (loss coefficients referred to the enthalpy drop in the group)

Loss increase along turbine	Calculated without leakage	Calculated with leakage	Difference
Downstream of stator 1	1.6%	1.6%	–
Downstream of rotor 1	3.8%	5.0%	+1.2%
Downstream of stator 2	5.6%	7.4%	+1.8%
Downstream of rotor 2	8.8%	12.0%	+3.2%

The comparison of spanwise distribution of enthalpy losses in subsequent blade rows and stages calculated without and with the tip leakage is presented in Figure 31. The stage loss coefficient does not take into account the leaving energy loss. Stator losses are calculated in the middle of the axial gaps, whereas the rotor and stage losses are calculated 45% of the axial chord downstream of the trailing edge. Expressions used to calculate stator, rotor and stage losses are enclosed in Appendix. The region of accumulation of leakage losses is located near the endwall. The comparison of loss curves clearly shows that the tip leakage over the shroud reduces the tip passage vortex in the rotor but intensifies secondary flows in the downstream stator. The level of losses in stage 2 is higher than in that in stage 1 due to non-uniformities of flow parameters at the exit from stage 1 – this refers both to the calculations without and with the leakage flow. The flow losses in subsequent blade rows are accrued in Table 1, where the loss coefficients are related to the enthalpy drop in the entire two stage group. In the presented configuration (leakage flow rate 2.7%, leakage jet swirl angle at re-entry 80°), the calculated loss increase due to the tip leakage amounts to 1.2% in the first rotor, 0.6% in the second stator and 1.4% in the second rotor. Assuming similar pressure drops in each stage, the calculated loss increase due to the tip leakage can be estimated at about 4%, out of which 7/10 falls on the rotor region and 3/10 on the downstream stator region. These values can be considered characteristic for the investigated configuration and are subject to change with the changing leakage configuration. A detailed determination of loss components due to leakage through labyrinth seals in an LP turbine with diverging endwalls can be found in a numerical work [38]. For a typical labyrinth seal geometry used in these investigations 19% of the total loss due to the tip leakage falls on the labyrinth region, 47.5% on the mixing region downstream of the rotor trailing edge, 12.5% on the downstream blade row,

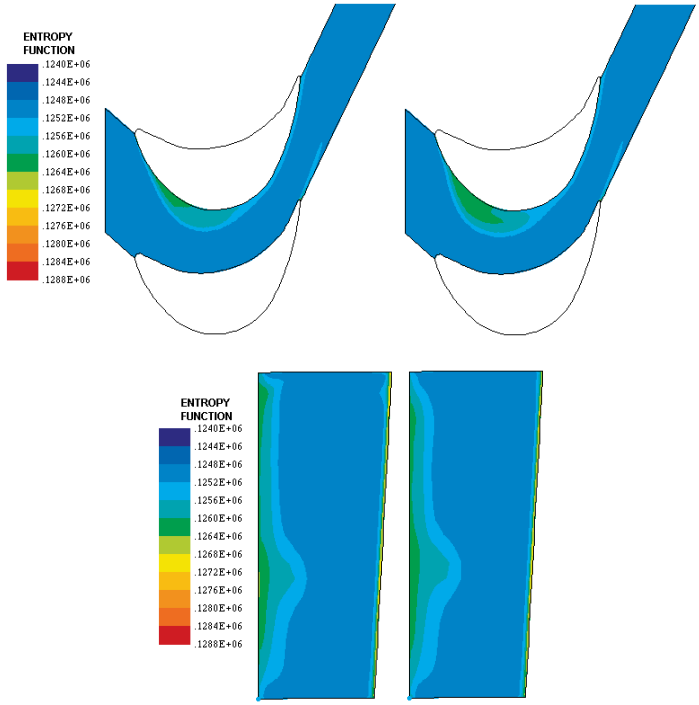

Figure 32. Entropy function contours in the blade-to-blade plane of the first rotor 10% blade height from the hub (top) and at the rotor trailing edge (bottom) for leakage mass flow rate 1% (top) and 3% (bottom)

whereas 19% are step losses, and the remaining losses are due to friction against the shroud. Reducing the clearance size (and leakage flow rate) decreases mixing losses, increasing the contribution of other components of the overall leakage loss.

Tip leakage has an effect on flow in the rotor where it is originated (first rotor), as well as in subsequent blade rows. Changes in the first rotor and in the downstream blade rows depend on the leakage flow rate and its direction at the re-entry to the blade-to-blade passage. Besides changes in the downstream mixing losses, also changes in the development of secondary flows and separation zone can be expected. These effects can be observed from Figure 32 showing entropy function contours in the first rotor 10% of the blade height from the hub and at the rotor trailing edge for two leakage flow rates 1% and 3% (of the stator mass flow rate). Due to the reduction of the mean axial velocity in the blade-to-blade passage and locally increased incidence at the rotor blade, the size of the separation zone increases with the increasing leakage flow rate, thus increasing separation losses. As the tip leakage flow helps to remove the tip boundary layer fluid from the blade-to-blade passage upstream of the rotor, the development of secondary flows at the tip is retarded, as a result of which the extension of secondary flow zone is reduced and secondary flow losses are decreased at the tip with the increasing leakage flow rate.

Figure 33 shows the comparison of entropy function contours downstream of the second stator, first comparing the results for two tip leakage jet flow rates 1% and 3% (at the tip leakage jet swirl angle 0°), and then for three leakage jet swirl angles

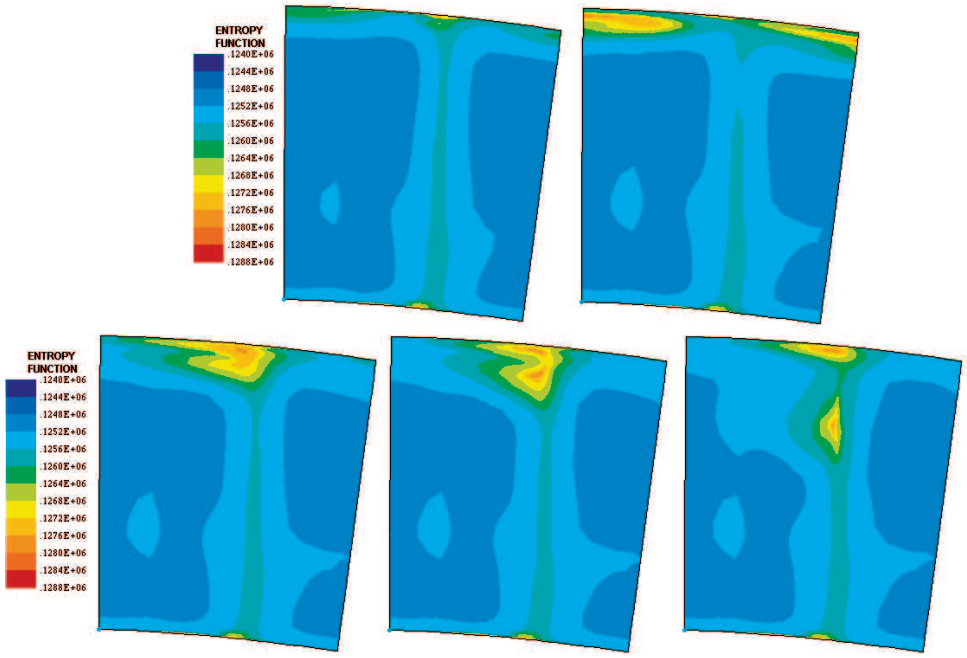

Figure 33. Entropy function contours in the normal plane downstream of the second stator: tip leakage jet flow rate 1% and 3%; swirl angle 0°, meridional angle −90° (top); tip leakage jet flow rate 3%; swirl angle 40°, 60° and 80°, meridional angle −90° (bottom)

40°, 60° and 80° (at a 3% tip leakage mass flow rate). The recirculating flow in the tip region of the downstream stator is intensified with the increasing leakage jet flow rate and swirl angle. The loss centre moves towards the mid-span and the losses in the downstream stator are increased. Reduction of leakage jet direction is a method of decreasing shroud leakage losses and raising the efficiency of turbine stages, [46].

8. Unsteady interactions in the region of tip leakage over unshrouded blades

Unsteady interactions were investigated using the solver FlowER. The calculations were made in a single passage of each blade row of the investigated stage group with the help of time-space periodicity conditions described in [47, 48]. A three-row group of stator-rotor-second stator of the Aachen model air turbine with short-height blading and reaction profiles, [49], was selected as an object of investigations. In nominal conditions this system operates at the inlet overpressure of 1.54bar, inlet temperature 309.2K, mass flow rate 6.8kg/s, rotor rotational speed 3500rev/min. The characteristic dimensions of the cascades are: blade span/chord – 0.89 (stators), 0.92 (rotor), pitch/chord – 0.86 (stators), 0.76 (rotor). The calculations were carried out for tip clearances above unshrouded rotor blades of size 0.4 and 1.0mm, on an H-type grid of $76 \times 72 \times 100$ elements in each blade row with the turbulence model of k-ω SST.

Figure 34 illustrates the transport of a stator wake through the mid-span of the rotor cascade, showing the entropy function contours at four instants of unsteady flow.

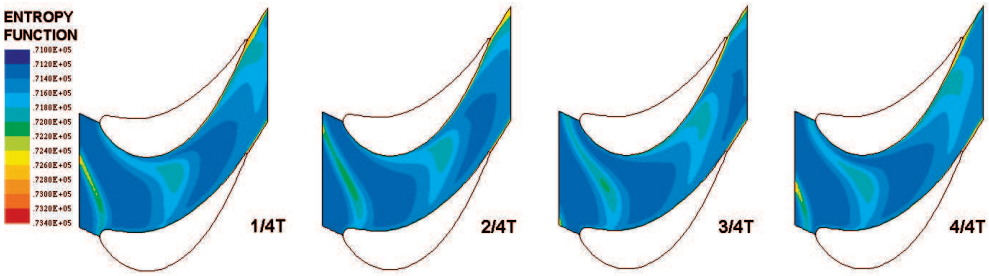

Figure 34. Instantaneous entropy function contours in the rotor at the mid-span in unsteady flow

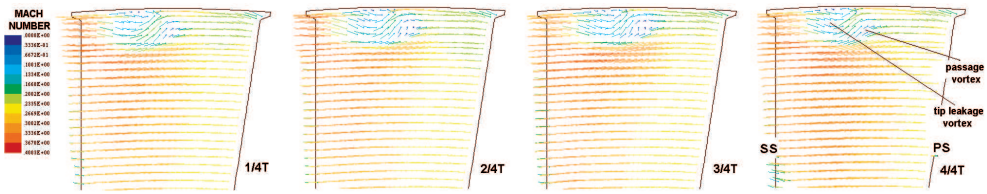

Figure 35. Instantaneous velocity vectors at the rotor trailing edge in unsteady flow coloured by Mach number

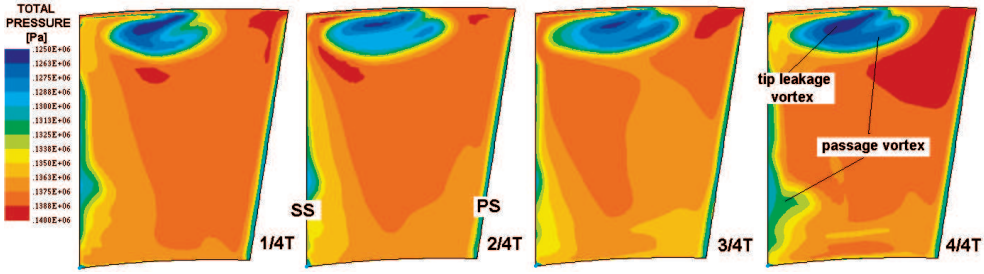

Figure 36. Instantaneous total pressure contours at the rotor trailing edge in unsteady flow

The effects of transport of two-dimensional wakes through the downstream cascade, including the effect of negative jet, periodic increase of turbulent fluctuations and changes in location of the laminar-turbulent transition are explained in [48, 50–54] where the wake transport along the separation zone and through the secondary flow zone was investigated. Due to the fact that the passing wakes move the incidence at the rotor blade towards the suction side, periodic reduction of intensity of the passage vortices and suction side separation was observed.

Velocity vectors and total pressure contours at the rotor trailing edge at subsequent instants within the period of unsteady flow are presented in Figures 35 and 36. It follows from the comparison of the pictures that periodic changes in size of the tip leakage vortex are less significant that those of the passage vortices both at the tip and hub endwall. This confirms earlier numerical results (Figure 13) that local changes of incidence angle are more important for the development of passage vortices. In the course of interaction of the stator wake the intensity of the passage vortices is reduced and the loss centre of the tip passage vortex remains closer to the endwall and pressure side of the blade. This tendency is in a qualitative agreement with the experimental results from the same model turbine presented in [55].

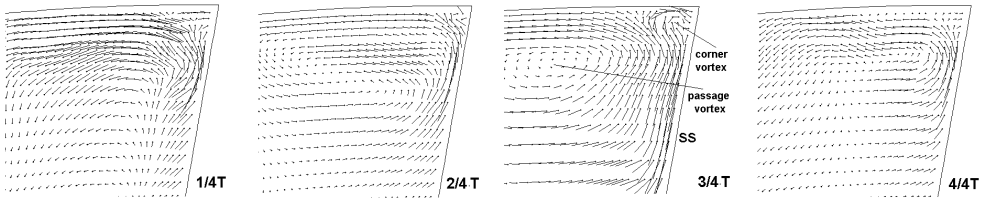

Figure 37. Instantaneous secondary flow vectors in the second stator 40% axial chord downstream of the leading edge in unsteady flow

The velocity defect impinging the rotor blade is not uniform span-wise. In the secondary flow dominated regions, the radial velocity and additional components of the swirl and axial velocity occur in the wake. These effects are relatively week downstream of the first stator with a small contribution of secondary flow losses in the overall loss balance. The transport of stator wakes can then be regarded as the passage of two-dimensional wakes skewed span-wise due to different convection velocities at the tip and hub. Quite contrary to that picture, the rotor wake has a clearly three-dimensional structure in the upper part of the channel dominated by the tip leakage vortex. Segmentation of this structure at the downstream stator leading edges and its further transport through the stator has a very complex nature. Figure 37 illustrates instantaneous secondary flow vectors in the upper part of the stator in a section located 40% of the axial chord downstream of the leading edge. The pictures exhibit the presence of a pulsating recirculating flow that encompasses the tip endwall boundary layer and segments of the co-rotating tip leakage vortex cut by the stator leading edge. This recirculating flow, leading to the formation of the pulsating passage vortex, is driven by the periodically changing span-wise pressure gradients at the blade surfaces near the tip endwall caused by locally non-nominal incidence at the blade, similar to that depicted in Section 7, Figures 26 and 27. Besides, in the tip endwall/suction side corner a pulsating vortex is observed originating from the reverse cross-flow from the stagnation point moved onto the suction surface at the time of interaction with the tip leakage vortex. This vortex is also fed downstream by the tertiary vortex structure due to separation of the recirculating flow from the endwall. At an instant free from interaction with the tip leakage the size of the passage vortex is reduced. The corner vortex disappears as the incidence at the stator blade turns near-nominal then. It can be deduced from Figure 37 that this instant is denoted as 4/4T. Due to a large size of the tip leakage vortex (together with the passage vortex) referred to the blade-to-blade distance, the time of interaction within the period of unsteady flow is longer than that of lack of interaction.

The kinetic energy of the tip leakage vortex is in large part dissipated during its transport in the structure of the stator passage vortex. Figure 38 illustrates instantaneous total pressure and entropy function contours at the trailing edge of the second stator in four instants of unsteady flow. The remains of the tip leakage vortex structure can be recognised at the trailing edge, especially at instants 3/4T and 4/4T, as regions of high total pressure in the upper part of the channel near the suction surface. Dissipation of the secondary kinetic energy of the tip vortex is pronounced by the increased entropy function in this part of the channel. Along the channel, the loss centre moves diagonally towards the suction surface and mid-span

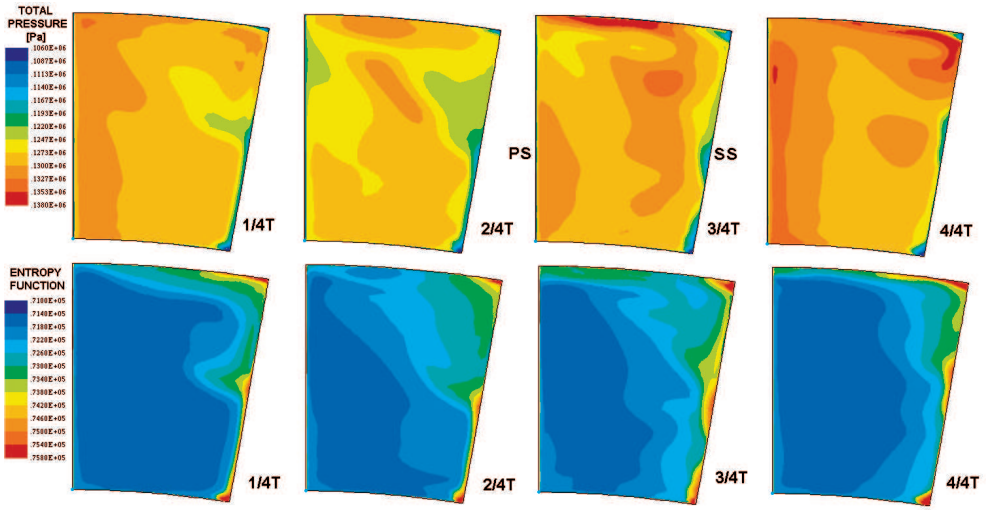

Figure 38. Instantaneous total pressure and entropy function contours at the second stator trailing edge in unsteady flow

sections as shown in [56]. The area distributions of total pressure and entropy function are subject to considerable changes within the period of unsteady flow. Oscillations due to interaction of the rotor wake in the lower part of the channel are smaller, but can also be recognised, especially in the region of hub secondary flow.

Only general tendencies in the process of unsteady interaction of three-dimensional wakes are pointed out in this paper. More detailed analysis will be possible after further developments of the flow solver, particularly concerning the adaptive grid generation.

9. Conclusions

The sources of flow losses in connection with the tip leakage over shrouded and unshrouded rotor blades were investigated. The theoretical analysis of dissipative process enables the evaluation of leakage losses and determination of parameters that have an effect on the level of loss. Making use of a number of simplifying assumptions and a model of lost secondary kinetic energy, leakage loss correlations were obtained. Validation on experimental cascades shows that these correlations can describe relatively well the leakage losses.

The effects of geometrical and flow parameters on the development of flow losses in the leakage-dominated region as well as on the interaction of tip leakage flow with secondary flows were also investigated using a 3D RANS solver. In the case of unshrouded free-tip blades, an increase of the tip gap size was found to increase the intensity and size of the tip leakage vortex, decrease the size of the tip passage vortex. The intensity of the passage vortex however increases with the increased flow turning in the cascade and when the incidence at the rotor blade is moved onto the pressure surface – both in the case of tip and hub vortices. The relative motion of the blade tips and endwall acts to considerably reduce the tip leakage and tip passage vortex.

Main properties of interaction of the shroud leakage with the main flow and secondary flows were presented. The shroud leakage helps to remove the low-energy

endwall boundary layer into the leakage slots, which retards the development of secondary flows in the current blade row. As compared to the case of no leakage calculations, the leakage flow may locally change the incidence at the blade onto the pressure side and increase the extension of the suction side separation zone. Unlike the leakage over unshrouded blades, the shroud leakage does not form a vortex structure on the re-entry to the blade-to-blade passage, but an axisymmetric mixing zone. The mixing processes are hardly accomplished in the rotor region. The inflow of the leakage stream onto the suction side of the downstream stator and local span-wise pressure gradients at the stator blades induce a strong recirculating flow in the stator. This recirculating flow rolls up both the low-energy endwall boundary layer fluid and high-energy mixing zone of the shroud leakage and gives rise to the formation of an intensive tip passage vortex in the stator. Large part of the total pressure surplus in the leakage region is dissipated in the stator channels. However, the remains of the leakage can still be recognised in the exit section as regions of increased total pressure.

An additional source of loss is unsteady transport of wakes through the downstream blade row. Transport of a two-dimensional stator wake leads to significant oscillations in size of the secondary flow zones and suction side separation, which can be explained by local changes of the inlet angle during the time of interaction with the passing wakes. Oscillations of flow parameters in the tip leakage region are less important. Particularly complex is downstream transport of three-dimensional rotor wakes, which include the tip leakage vortex. The structure of the tip leakage vortex segmented by the leading edges of the downstream stator is found within the pulsating recirculating flow, from which a pulsating passage vortex is formed in the stator. In the tip endwall/suction side corner another pulsating counter-rotating vortex is observed originating from the endwall cross-flow from the stagnation point moved onto the suction side. Large part, but not all of the secondary kinetic energy of the tip leakage vortex is dissipated in the stator channels.

Appendix

In this appendix, enthalpy losses in the stator, rotor and stage are defined. The definitions are gathered in Table A1 and are easily explained with the help of Figure A1 showing an enthalpy-entropy diagram of the expansion process in a turbine stage.

Table A1. Enthalpy losses in the stator, rotor and stage

Stator loss	$\xi_1 = (h_1 - h_{1s})/(h_{0T} - h_{1s})$
Rotor loss	$\xi_2 = (h_2 - h_{2s})/(h_{1T} - h_{2s})$
Stage loss (without exit energy = stator + rotor loss)	$\xi_{12} = (h_2 - h_{2s'})/(h_{0T} - h_{2s'})$
Stage loss (with exit energy = stator + rotor loss + exit energy)	$\xi_{12c} = (h_{2T} - h_{2s'})/(h_{0T} - h_{2s'})$

References

[1] Gardzilewicz A and Marcinkowski S 1995 *ASME PWR* **28** (3) 349

[2] Marcinkowski S 1998 *Rep. Inst. Fluid Flow Machinery, Gdansk* **292** 98 (in Polish)

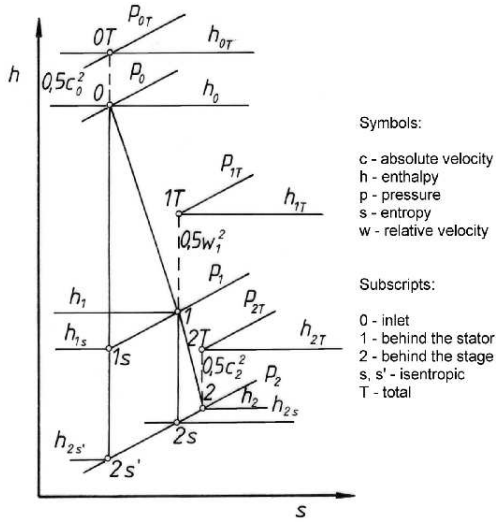

Figure A1. Enthalpy-entropy diagram for a turbine stage

[3] Denton J D 1993 *Trans. ASME J. Turbomachinery* **115** 621
[4] Bindon J P 1987 *I. Mech. E. Paper* **C273** 87
[5] Bindon J P 1989 *Trans. ASME J. Turbomachinery* **111** 257
[6] Sjolander S A and Amrud K K 1987 *Trans. ASME J. Turbomachinery* **109** 237
[7] Sjolander S A and Cao D 1995 *Trans. ASME J. Turbomachinery* **117** 578
[8] Yaras M I, Zhu Y and Sjolander S A 1989 *Trans. ASME J. Turbomachinery* **111** 276
[9] Graham J A H 1986 *Trans. ASME J. Engng Gas Turbines Power* **108** 38
[10] Xiao X, McCarter A A and Lakshminarayana B 2000 *ASME Pap.* 2000-GT-0476
[11] Xiao X, McCarter A A and Lakshminarayana B 2000 *ASME Pap.* 2000-GT-0477
[12] Sjolander S A 1997 *VKI LS* 1997-01
[13] Moore J and Tilton J S 1988 *Trans. ASME J. Turbomachinery* **110** 18
[14] Yaras M I and Sjolander S A 1990 *Trans. ASME J. Turbomachinery* **112** 609
[15] Tallman J and Lakshminarayana B 2000 *ASME Pap.* 2000-GT-0514
[16] Tallman J and Lakshminarayana B 2000 *ASME Pap.* 2000-GT-0516
[17] Yamamoto A 1988 *Trans. ASME J. Turbomachinery* **110** 329
[18] Yamamoto A 1989 *Trans. ASME J. Turbomachinery* **111** 264
[19] Yamamoto A, Matsyunuma T and Outa E 2001 *Three-dimensional Flows and Losses in an Ultra-highly Loaded Turbine*, Rep. National Aerospace Lab., Tokyo, Japan
[20] Chan J K K, Yaras M I and Sjolander S A 1994 *ASME Pap.* 94-GT-250
[21] Moore J G, Schorn S A and Moore J 1996 *Trans. ASME J. Turbomachinery* **118** 622
[22] Heyes F J G, Hodson H P and Dailey G M 1992 *Trans. ASME J. Turbomachinery* **114** 643
[23] Lampart P, Gardzilewicz A, Szymaniak M, Kurant B, Banaszkiewicz M and Malec A 2003 *Trans. IFFM* **114** 19
[24] Boletis E and Sieverding C H 1991 *Trans. ASME J. Turbomachinery* **113** 1
[25] Morphis G and Bindon J P 1994 *ASME Pap.* 94-GT-481
[26] Yaras M I and Sjolander S A 1992 *Trans. ASME J. Turbomachinery* **114** 204
[27] Ainley D G and Mathieson G C R 1951 *ARC R&M Rep.* 2891
[28] Dunham J and Came P M 1970 *Trans ASME, J. Eng. Power* **92** (3) 252
[29] Kacker S C and Okapuu U 1982 *Trans. ASME J. Engng Power* **104** 111
[30] Yaras M I and Sjolander S A 1992 *Trans. ASME J. Turbomachinery* **114** 652

[31] Dishart P T and Moore J 1990 *Trans. ASME J. Turbomachinery* **112** 599
[32] Kim B N and Chung M K 1997 *Trans. ASME J. Turbomachinery* **119** 399
[33] Heyes F J G and Hodson H P 1993 *Trans. ASME J. Turbomachinery* **115** 373
[34] Yaras M I, Sjolander S A and King R J 1992 *Trans. ASME J. Turbomachinery* **114** 660
[35] Yershov S and Rusanov A 1997 *The Application Package FlowER for the Calculation of 3D Viscous Flows Through Multi-stage Machinery*, Certificate of Registration of Copyright, Ukrainian State Agency of Copyright and Related Rights, Kiev
[36] Yershov S, Rusanov A, Gardzilewicz A, Lampart P and Świrydczuk J 1998 *TASK Quart.* **2** (2) 319
[37] Lampart P, Świrydczuk J and Gardzilewicz A 2001 *TASK Quart.* **5** (2) 191
[38] Gier J, Stubert B, Brouillet B and de Vito L 2003 *ASME Pap.* GT2003-38025
[39] Kosowski K 1995 *The Optimum Values of the Main Design Parameters of Turbine Stages. The Generalised Design Method of Turbine Stages*, Zeszyty Naukowe Politechniki Gdańskiej, Budownictwo Okrętowe LXII, No. 528 (in Polish)
[40] Lampart P, Gardzilewicz A, Yershov S and Rusanov A 2000 *ASME Pap.* IJPGC2000-15004
[41] Lampart P, Gardzilewicz A, Yershov S and Rusanov A 2001 *J. Thermal Science* **10** (3) 198
[42] Lampart P, Yershov S, Rusanov A and Szymaniak M 2004 *ASME Pap.* GT2004-53882
[43] Gibboni A, Menter J R, Peters P, Wolter K, Pfost H and Breisig V 2003 *ASME Pap.* GT2003-38722
[44] Błażko E and Lidke M 1996 *TUR-96 – Computer Programme for Heat-and-Flow Calculations of Turbine Blading Systems of Given Geometry*, Opr. Diagnostyka Maszyn sp. z o.o., Gdansk, No. 21/96 (in Polish)
[45] Peters P, Breisig V, Giboni A, Lerner C and Pfost H 2000 *ASME Pap.* 2000-GT-478
[46] Wallis A M, Denton J D and Demargne A A J 2000 *ASME Pap.* 2000-GT-475
[47] Rusanov A V and Yershov S V 1977 *Proc. Int. Conf. Modelling and Design in Fluid-Flow Machinery*, Gdansk, Poland, pp. 153–160
[48] Lampart P, Rusanov A, Yershov S, Świrydczuk J and Gardzilewicz A 1999 *Cieplne Maszyny Przepływowe* **115** 285
[49] Walraevens R and Gallus H E 1999 *Rep. Institute of Jet Propulsion and Turbomachinery*, RWTH Aachen
[50] Kerrebrock J L and Mikolajczak A A 1970 *Trans. ASME J. Engng Power* **92** 359
[51] Mayle R E and Dullenkopf K 1989 *Trans. ASME J. Turbomachinery* **111** 188
[52] Wierciński Z 1999 *Wake Induced Laminar-turbulent Transition in the Boundary Layer*, Zeszyty Naukowe IMP PAN, No. 499/1450/99 (in Polish)
[53] Elsner W, Vilmin S, Drobniak S and Piotrowski W 2004 *ASME Pap.* GT2004-53757
[54] Lampart P 2006 *Numerical Investigations of Aerodynamics of Turbine Blading Systems*, Zeszyty Naukowe IMP PAN (in print; in Polish)
[55] Stephan B, Gallus H and Niehuis R 2000 *ASME Pap.* 2000-GT-613
[56] Lampart P, Rusanov A, Yershov S, Gardzilewicz A and Badur J 1999 *Proc. VI ERCOFTAC Seminar and Workshop on 3D Turbomachinery Flow Prediction*, Aussois, France

View publication stats